



# Structured sulphur trioxide splitting catalytic systems and allothermally-heated reactors for the implementation of Sulphur-based thermochemical cycles via a centrifugal solar particle receiver

Christos Agrafiotis<sup>a,\*</sup>, Dennis Thomey<sup>b</sup>, Lamark de Oliveira<sup>a</sup>, George Karagiannakis<sup>c</sup>, Nikolaos I. Tsongidis<sup>c,d</sup>, Chrysoula Pagkoura<sup>c</sup>, Gözde Alkan<sup>e</sup>, Martin Roeb<sup>a</sup>, Christian Sattler<sup>a,f</sup>

<sup>a</sup> DLR - Deutsches Zentrum für Luft, und Raumfahrt / German Aerospace Center, Institute of Future Fuels, Linder Höhe, 51147, Cologne, Germany

<sup>b</sup> DLR - Deutsches Zentrum für Luft, und Raumfahrt / German Aerospace Center, Institute of Future Fuels, Professor-Rehm-Strasse 1, 52428 Juelich, Germany

<sup>c</sup> Centre for Research and Technology Hellas / Chemical Processes and Energy Resources Institute, (CERTH/CPERI), 6th km Charilaou-Thermi road, 57001, Thessaloniki, Greece

<sup>d</sup> Department of Chemical Engineering, Aristotle University of Thessaloniki (AUTH), 54124, Thessaloniki, Greece

<sup>e</sup> DLR - Deutsches Zentrum für Luft, und Raumfahrt / German Aerospace Center, Institute of Materials Research, Linder Höhe, 51147, Cologne, Germany

<sup>f</sup> RWTH Aachen University Faculty of Mechanical Engineering, 52056 Aachen, Germany

## ARTICLE INFO

### Keywords:

Sulphur trioxide splitting  
Iron oxide catalysts  
Structured reactors  
Sulphur thermochemical cycles  
Concentrated solar energy

## ABSTRACT

Catalytic sulphur trioxide splitting is the highest-temperature (850–900 °C), endothermic step of several sulphur-based thermochemical cycles targeted to production of hydrogen or solid sulphur. The demonstrated capability of centrifugal particle solar receivers of heating particle streams at such temperatures, can allow for “allothermal” implementation of this step via the enthalpy of such particle streams in a catalytic shell-and-tube reactor/heat exchanger decoupled from a solar receiver. In this context, SO<sub>3</sub> splitting catalytic systems shaped to spherical particles and flow-through honeycombs and foams were prepared and tested. Long-term (100–950 h) experiments with catalyst-coated SiC honeycombs demonstrated that oxide-supported Pt catalysts suffered from low conversion and severe deactivation at 650 °C, contrary to Fe<sub>2</sub>O<sub>3</sub>-coated ones. Fe<sub>2</sub>O<sub>3</sub>-coated SiC foams demonstrated reproducible near-equilibrium conversion at 850 °C, under a broad range of sulphuric acid flow rates, combined with minute pressure drop even under high catalyst loadings (35–45 wt %) being thus in principle suitable for eventual pressurized operation.

## 1. Introduction

Thermochemical cycles of the sulphur family were initially coined as a route to produce hydrogen via water splitting; they are a series of consecutive chemical reactions among which sulphur is recycled, appearing at changing oxidation states in different compounds. The chemistries of the most studied ones, the Sulphur Iodine (SI) cycle introduced by General Atomics in the mid-seventies [1] and the Hybrid Sulphur (HyS) cycle set forth and investigated by Westinghouse Electric corporation [2], are described in Table 1, together with the indicative temperatures required per step according to current state-of-the-art. However, as also proposed by General Atomics [3], they can both be modified to produce Solid Sulphur (SoSu) if their common, endothermic sulphuric acid dissociation/sulphur trioxide splitting (SAD-STs)

reactions (1a, 1b) are followed by the disproportionation (5) of therein produced SO<sub>2</sub> into sulphuric acid and elemental sulphur. The latter, can then be employed as a fuel, by being combusted in air (reaction 6), producing on-demand high-temperature heat and SO<sub>2</sub>. The combustion-produced SO<sub>2</sub> can be converted back into sulphur and H<sub>2</sub>SO<sub>4</sub> via reaction (5), thereby closing the cycle [4]. Hence, whereas, in the HyS and SI cycles the net reactions' sum in Table 1 is water splitting to hydrogen and oxygen [5], in the SoSu cycle the “net” mass balance of the reactions is zero; the valuable outcome is the high-quality heat generated via the combustion of sulphur that can result in temperatures in excess of 1200 °C and hence employed in gas turbines for efficient combined cycle power generation. The SoSu cycle is also adaptable to flexible, “open cycle”-operation (i.e. resulting in a non-zero net mass balance): material feedstocks (H<sub>2</sub>SO<sub>4</sub>, S, SO<sub>2</sub>) from/to sulphuric acid

\* Corresponding author.

E-mail address: [christos.agrafiotis@dlr.de](mailto:christos.agrafiotis@dlr.de) (C. Agrafiotis).

<https://doi.org/10.1016/j.apcatb.2022.122197>

Received 8 September 2022; Received in revised form 15 November 2022; Accepted 17 November 2022

Available online 19 November 2022

0926-3373/© 2022 Elsevier B.V. All rights reserved.

**Table 1**

Chemical reactions of the Hybrid Sulphur (HyS), Sulphur-Iodine (SI) and Solid Sulphur (SoSu) thermochemical cycles.

Cycle	Cycle Reactions			Temperature (°C)	ΔH <sup>0</sup> (kJ/ mol)
HyS	Sulphuric acid dissociation	1a	H <sub>2</sub> SO <sub>4</sub> (g) → H <sub>2</sub> O(g) + SO <sub>3</sub> (g)	450–500	+ 98
	SO <sub>3</sub> splitting	1b	SO <sub>3</sub> (g) → SO <sub>2</sub> (g) + ½ O <sub>2</sub> (g)	650–950	+ 99
	Electrolysis	2	2 H <sub>2</sub> O + SO <sub>2</sub> → H <sub>2</sub> SO <sub>4</sub> + H <sub>2</sub> (g)	50	
	Anode	2a	SO <sub>2</sub> + 2 H <sub>2</sub> O → H <sub>2</sub> SO <sub>4</sub> + 2 H <sup>+</sup> + 2e <sup>-</sup>		
	Cathode	2b	2 H <sup>+</sup> + 2 e <sup>-</sup> → H <sub>2</sub>		
SI	Bunsen reaction	3	2 H <sub>2</sub> O + SO <sub>2</sub> + I <sub>2</sub> → H <sub>2</sub> SO <sub>4</sub> + 2HI	25–125	- 75
SoSu	HI decomposition	4	2HI → I <sub>2</sub> (g) + H <sub>2</sub> (g)	125 - 725	+ 12
	Disproportionation	5	2 H <sub>2</sub> O(l) + 3SO <sub>2</sub> (g) → 2 H <sub>2</sub> SO <sub>4</sub> (aq) + S(s)	50–200	-260
	Sulphur combustion	6	S(l) + O <sub>2</sub> (g) → SO <sub>2</sub> (g)	500–1500	-300

production plants and/or sour gas and crude oil processing plants [6] can be used/supplied, since elemental sulphur is nowadays nearly exclusively produced worldwide from the latter as an involuntary by-product to reduce SO<sub>x</sub> emissions from the combustion of these fossil fuels [7]. Solid S, liquid H<sub>2</sub>SO<sub>4</sub> and SO<sub>2</sub> in liquid form, can all be long-term stored economically under ambient conditions.

The common to the three cycles steps of thermal sulphuric acid dissociation (SAD) first to water (steam) and sulphur trioxide (SO<sub>3</sub>) and subsequent catalytic sulphur trioxide splitting to sulphur dioxide (SO<sub>2</sub>) and oxygen are performed experimentally in combination, with heat from the same heat source: a reservoir containing concentrated sulphuric acid is heated above the solution's boiling point and the vapours produced are led first through a medium-temperature zone where H<sub>2</sub>SO<sub>4</sub> is dissociated stoichiometrically into steam and SO<sub>3</sub> and then through a catalytic reactor at higher temperatures where the STS step is implemented. The latter is actually the highest-temperature -  $\approx$  850–950 °C - endothermic reaction step of the three cycles. To abide with the requirements of "clean" production, the heat necessary for the implementation of this step needs to be supplied entirely from renewable or carbon-neutral energy sources. Indeed, the interest on such water-splitting cycles was initiated by the nuclear energy sector and focused on coupling the endothermic SAD-STs step to very high temperature nuclear reactors (VHTR); helium (He) gas coolant of VHTRs available at temperatures in the range of 950 °C was conceived as the heat transfer fluid (HTF) providing "allothermally" the high-temperature heat for the endothermic SAD-STs steps in a heat exchanger/chemical reactor [8]. Whereas this approach is still pursued today in countries utilizing nuclear power to cover their energy needs like Japan, China and U.S.A. [9–11], the climate change societal debate brought Concentrated Solar Energy (CSE) into play as a high temperature heat source. In this context, SAD-STs was explored employing various CSE-heated reactor concepts like tubular reactors absorbing solar radiation on their external surface and transferring the heat to their internal one containing the catalyst wherein the reactant gas mixture flows (General Atomics, [12]) or directly irradiated stationary volumetric solar receivers/reactors shaped to porous structures like foams and honeycombs from silicon carbide (SiC) coated with suitable oxide catalysts, with the process gas flowing through the porous absorber/reactor volume (DLR, [13]). Operational issues encountered during the scale-up of the latter concept

like high re-radiation losses from the structured bodies' front irradiated surface and limited high-temperature length achieved along the porous catalyst-coated receiver, together with the necessity for a window, were judged to limit its scalability [14].

The demonstrated capability of (developed and patented by DLR) centrifugal particle solar receivers (Fig. 1a) of heating flowing solid particle streams at temperature levels of the order of 900–950 °C [15] can render the implementation of the SAD-STs steps feasible "allothermally" via the enthalpy of solar receiver-heated solid particles in a catalytic reactor/heat exchanger spatially decoupled from the receiver (Fig. 1b, c). The concept can be considered analogous to that construed for coupling sulphur water splitting thermochemical cycles to VHT nuclear reactors [16], essentially replacing Helium with a high-temperature solar-heated moving particles stream. Such an approach has the following advantages:

- Elimination of design, engineering and operating complexities of solar receiver/reactors having to address at the same time efficient collection of solar energy and its effective transfer to the reacting feedstock of sulphuric acid vapours that have to come to close proximity, requiring hence expensive materials with a combination of exceptional properties like solar irradiation absorbance, refractoriness, corrosion resistance and catalytic activity, as well as of scale-up limitations due to the size of the receiver-reactor and the unavoidable need for windows given the controlled reaction atmosphere.
- The "ground level" operation of a SAD-STs reactor instead of on atop of a solar tower can much more easily exploit all industrially practiced developments and technical solutions of "traditional" sulphuric acid-relevant chemical engineering: catalytic designs, heat exchange schemes and SO<sub>x</sub> emissions capture/neutralisation approaches.
- Particles can be used to sensibly store solar heat in a hot storage system (tank) and thus employed also off-sun to thermally drive the SAD-STs reaction scheme in cases of either diurnal solar radiation interruption (e.g. cloud passages) or overnight, guaranteeing hence SO<sub>2</sub> availability and consequent hydrogen or solid sulphur production around the clock.

Within this context, initially the idea of introducing catalytically active elements into the solid particles composition and employing the particles stream as a combined concentrated solar irradiation harvesting/moving catalyst bed medium was explored in our previous work [17]. The results concluded to the selection of an alternative shell-and-tube type, cascaded SAD-STs reactor/heat exchanger, its operation principle schematically depicted in Fig. 2. Therein, commercially available, inexpensive, catalytically inactive bauxite particles preheated in the solar receiver, will flow in the reactor's shell transferring their enthalpy to non-moving catalytic beds inside a number of tubes through which the H<sub>2</sub>SO<sub>4</sub> vapours flow upwards and are decomposed first to steam and SO<sub>3</sub> and subsequently to SO<sub>2</sub> and oxygen [18]. Such a configuration can take advantage of the know-how and progress made so far with similar catalytic porous structures in the reactor/receivers already employed [14,19], being at the same time waived of the requirement and associated complexities of efficient solar irradiation collection within the same volume where the catalytic reaction takes place.

A further argument advocating the selection of the specific configuration stems from the feasibility of integrated operation considering the entire plant (Fig. 1d, e). In general, full SO<sub>3</sub> conversion is not achievable under the allowable operating reactor temperature and hence the reaction hot products gas stream contains SO<sub>2</sub>, O<sub>2</sub>, un-reacted SO<sub>3</sub> and H<sub>2</sub>O vapors. This mixture has to be cooled in order to allow SO<sub>2</sub> recovery and recycling of unreacted components. During cooling, un-reacted SO<sub>3</sub> rehydrates and condenses as H<sub>2</sub>SO<sub>4</sub> which, depending on its concentration level, may be routed back to either an H<sub>2</sub>SO<sub>4</sub> concentration section or a storage tank. The residual rich in SO<sub>2</sub> and O<sub>2</sub> gas

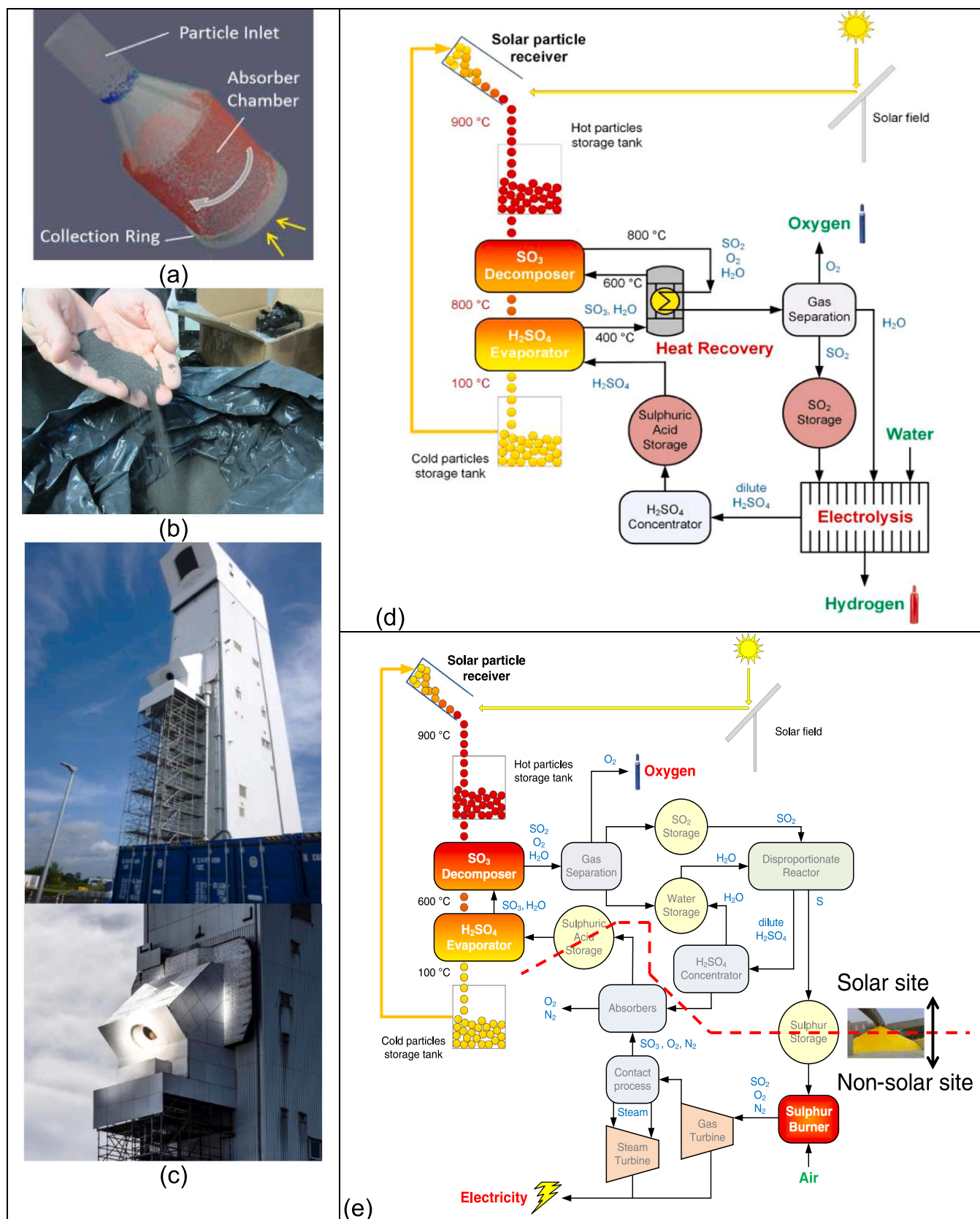


**Fig. 1.** (a) Centrifugal particle receiver operation principle [17]; (b) typical size of bauxite particles employed; (c) installation and operation of the receiver on Solar Tower Juelich under solar irradiation; (d), (e) indicative respective block diagrams of centrifugal particle receiver-driven hybrid- and solid sulphur-cycle plants [17].

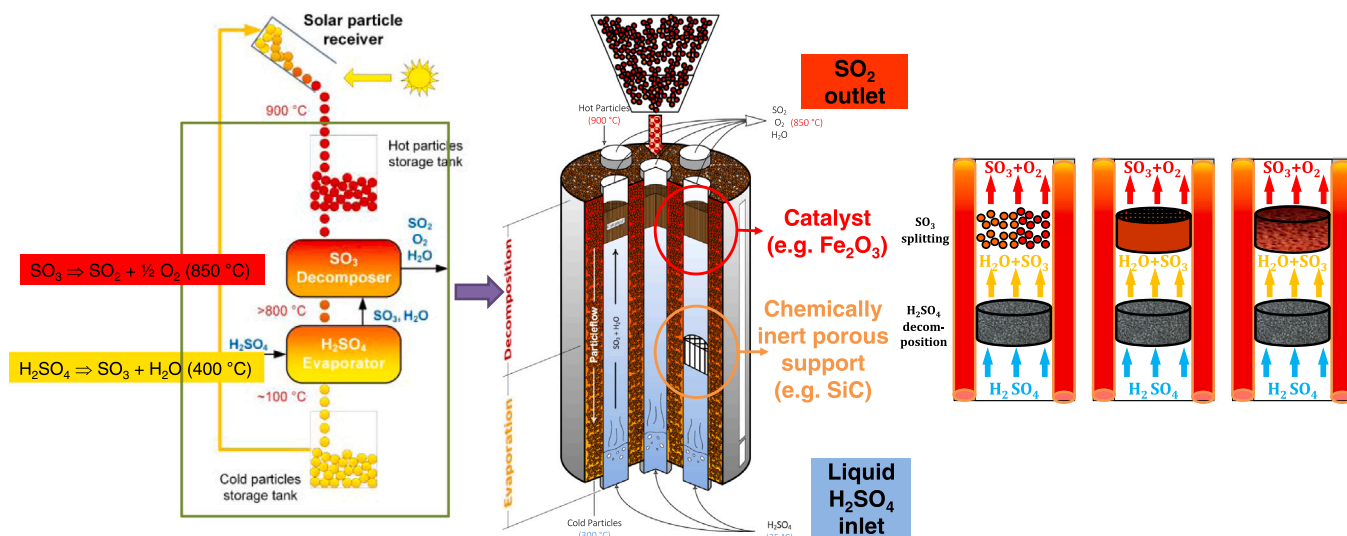


**Fig. 2.** Operation concept schematic of in-series SAD-STs reactor cascade heated allothermally with non-catalytic particles and various options for the catalytic bed section: particles (or small pellets), foams or honeycombs that can be either coated with or made partially or entirely of catalytic (iron) oxides; the lower, non-catalytic, thermal SAD region is filled with non-coated similar porous structures operating as flow distributors/homogenizers.

mixture needs to be separated prior to feeding  $\text{SO}_2$  to the next cycle step (Table 1), this being either the sulphuric acid electrolyzer (HyS cycle), the Bunsen reactor (SI cycle) or the disproportionation reactor (SoSu cycle).  $\text{SO}_2$  can be easily separated by condensation as well as by absorption with water as solvent due to its polarity. Both separation routes are favored at high pressures. It is therefore conceived that a pressurized  $\text{H}_2\text{SO}_4$  decomposition reactor will result in lower compression work in the following oxygen separation stages, in addition to providing for a more compact system design, with an in-principle affordable penalty in the achieved conversion of  $\text{SO}_3$  to  $\text{SO}_2$ . This fact advocates not only for decoupling the  $\text{SO}_3$  splitting reactor from the receiver since pressurized SAD-STs receiver/reactors are very challenging to be materialized especially in large-scale, but furthermore for the option of allothermally-heated shell-and-tube reactor concept since only the catalytic tubular chambers have to be designed for pressurized operation. In fact, an allothermal concept using solar-heated Helium that in turn was to be utilized as heat transfer medium in a pressurized shell-and-tube  $\text{SO}_3$  splitting reactor was proposed as early as 1983 by the inventor of the HyS cycle, Westinghouse Electric corporation. The reactor was construed as a non-moving packed bed of catalyst located in the shell-side, operating at 20 atm and achieving 67 %  $\text{SO}_3$  conversion while heated via Helium flowing through the tubes; however it was never materialized in a solar facility [20]. Pressurized SAD-STs reactors were also pursued by General Atomics [21] and SANDIA [22].

In this perspective, the power losses due to pressure drop of the reactant gaseous stream through the reactor's catalytic bed become important. Hence, "structured" catalytic reactors comprised of flow-through porous objects like honeycombs and foams with the catalyst particles "arranged" in space at the reactor level [23] rather than packed or fluidized catalytic particle beds where the catalyst particles are randomly distributed in space, can become a smart engineering alternative. Indeed, the inherent characteristics of ceramic honeycombs and reticulated foams such as high geometric surface area available for enhanced gas-solid contact, capability of accommodating high gas flow rates yet without a significant increase on pressure drop and facile deposition of functional coatings, especially when combined with special material properties like high thermal shock/corrosion resistance, thermal conductivity and mechanical strength offer an attractive alternative to packed beds for the implementation of gaseous-solid reactants at high temperatures [24]. Scale-up of well-geometrically defined, structured reactors is much easier than that of random systems, like packed particle/powder beds. The scale-up modularity becomes

especially beneficial in the specific case where thermal-only  $\text{H}_2\text{SO}_4$  evaporation and dissociation has to precede the catalytic  $\text{SO}_3$  splitting, since the lower part of the reactor's cascade can be comprised from non-catalytically-active similar porous structures acting as flow distributors/homogenizers. The catalytically active porous structures will constitute the top part of the cascade which the reactant gases will reach having been preheated throughout their flow upwards (Fig. 2). The corrosive nature of the liquids and gases employed have rendered the silicon carbide (SiC) family and in particular, its dense, silicon-infiltrated (or siliconized) version known with the abbreviation SiSiC [14,25], as the selection of choice for these parts for both regions.

Considering the state-of-the-art of  $\text{SO}_3$  splitting catalytic materials, extensive research by various groups has screened a large number of such catalysts, converging to either noble metals or transition metal oxides as the principal systems of choice [26]. If the former, expensive ones are to be avoided, the "next best" possible solution is single or mixed oxides of abundant transition metals [27], including principally iron oxide ( $\text{Fe}_2\text{O}_3$ ) or CuO-based compositions (e.g.  $\text{CuAl}_2\text{O}_4$ ), in many cases supported or dispersed with other oxides like silica [28,29] or even SiC [30], to improve their activity or longevity. Partial substitution of iron cations with chromium ones produced positive results: substitution of 10 % Cr in  $\text{Fe}_2\text{O}_3$  resulted in enhanced activity and also prevented catalyst deactivation during the  $\text{H}_2\text{SO}_4$  dissociation reaction [31]. Studies of the present authors corroborated the beneficial effect of Cr. A composition of  $\text{Fe}_{0.7}\text{Cr}_{1.3}\text{O}_3$  in particular, demonstrated activity not only substantially higher than  $\text{Fe}_2\text{O}_3$  and CuO but also close to that of the state-of-the-art yet highly costly Pt/ $\text{Al}_2\text{O}_3$  system [32]. Practically, all such oxide catalysts require temperatures between 800 and 950 °C to achieve conversions close to the equilibrium ones [33]. Metal vanadate-based catalytic formulations constitute an interesting alternative as they have demonstrated similar conversions at lower temperatures, 600–650 °C. However, their use imposes challenges as they need to be safely contained in partially molten stage [34,35] and, in general, are active under lower  $\text{SO}_3$  concentrations which implies the use of substantial amount of inert gas in the reaction mixture. On the other hand, by operating in their molten state exhibit superior activity vs. that of their solid-state counterparts since they capture  $\text{SO}_3$  gas as sulphate ions ( $\text{SO}_4^{2-}$ ) and efficiently convert to  $\text{SO}_2/\text{O}_2$  inside the liquid phase [36]. This mechanism is similar to that of the operation of industrial  $\text{V}_2\text{O}_5$ -based molten-phase catalysts for the reverse reaction of  $\text{SO}_2$  oxidation to produce sulphuric acid as demonstrated by in-situ Raman spectroscopy studies [37,38]. To address the issue of pressure drop

mentioned above, iron oxide, plain and doped with chromium [39] as well as Pt/Al<sub>2</sub>O<sub>3</sub> catalytic systems [40] were shaped and tested in the form of granules [41]. However, oxide catalysts and in particular made of Fe<sub>2</sub>O<sub>3</sub>, have been already manufactured to shaped structured objects like honeycombs and foams, but addressing different applications. Researchers of Corning Inc. have reported the manufacture of a honeycomb reactor for catalytic ethylbenzene dehydrogenation entirely from the catalyst material, iron oxide (Fe<sub>2</sub>O<sub>3</sub>), with such Fe<sub>2</sub>O<sub>3</sub>-based honeycombs extruded in various cell densities of up to 400 cpsi (cells per square inch). The rationale was exactly to incorporate these structures in a reactor/heat exchanger assembly in order to minimize thermal gradients while maintaining simultaneously low-pressure drop [42,43]. Therefore, in the present work targeted to the eventual incorporation of a scalable, modular robust catalytic system in a shell-and-tube reactor, the catalytic materials were long-term (100–950 h on-stream) tested as coated on SiC honeycombs and foams. Furthermore in order to investigate any favourable effect of increasing the quantity of the catalyst in the reactor bed, catalytic structures made entirely out of iron oxide were also prepared and comparatively tested: iron oxide spherical particles by CERTH [44] and iron oxide-made foams by DLR [45,46]. It should be stressed that the results are directly exploitable in all sulphur-based thermochemical cycles sharing the common SAD-STS step [47] irrespective of whether the high temperature source is solar or nuclear energy.

## 2. Materials and methods

The mixed oxide catalyst compositions were prepared in-house by CERTH as described previously [48] whereas commercial Fe<sub>2</sub>O<sub>3</sub> powder (supplier CERAMETEK, China, purity ≥ 99.5 %) was used for the preparation of catalytic structures employing only Fe<sub>2</sub>O<sub>3</sub> as the

transition metal oxide catalyst. Fe<sub>2</sub>O<sub>3</sub>-coated SiSiC honeycombs and foams were prepared by CERTH. The uncoated SiSiC segments - honeycombs of 25.4 mm diameter × 25.4 mm length, of 300 cells per square inch (cpsi) and foams of 25 mm diameter × 40 mm length, of 20 pores per linear inch (ppi) - were acquired from commercial suppliers (IBIDEN Co. Ltd, Japan and EngiCer S.A., Switzerland, respectively). Their porosity and pore size distribution are shown in Fig. 3a. Both have less than 2.0 % porosity and are characterized by pore size distribution curves of similar shape with mean pore diameters of 18.5 and 33.5 μm, respectively. These supports were subsequently coated via a “slurry dip coating” procedure similar to that used in the automotive exhaust catalytic aftertreatment community. Specifically, the dried ceramic supports were immersed in a stirred, stabilized, 30–40 wt % of fine hematite Fe<sub>2</sub>O<sub>3</sub> powder, aqueous slurry. The particle size distribution ( $d_{50} = 0.49 \mu\text{m}$ ;  $d_{90} = 10 \mu\text{m}$ ) of the powder was measured with a Malvern Mastersizer-X Low Angle Laser Light Scattering Analyzer/LALLS instrument and its specific surface area (5.79 m<sup>2</sup>/g) with the aid of a nitrogen adsorption porosimeter (Micromeritics ASAP 2000). Subsequent steps included the removal of excess slurry by vacuum to avoid over-loading and pore/channels blockage, drying and repetition of the procedure for as many times as needed to achieve the required loading; loading is defined as the (weight of the iron oxide deposited / weight of the uncoated foam support, in %). The coated specimens were finally calcined under air at 900 °C for 2 h to firmly adhere the coating onto the substrate. A similar approach was followed for the preparation of honeycombs coated with the other oxide catalyst tested, Fe<sub>0.7</sub>Cr<sub>1.3</sub>O<sub>3</sub>.

The committed long-term SAD-STS catalytic test rig at DLR depicted in Fig. 3b, has been extensively described in our previous relevant works [17,49]. All experiments were performed at atmospheric pressure and with ≈ 95 wt% concentrated sulphuric acid as reactant. Parametric studies involved variation of the reaction temperature and the feed flow

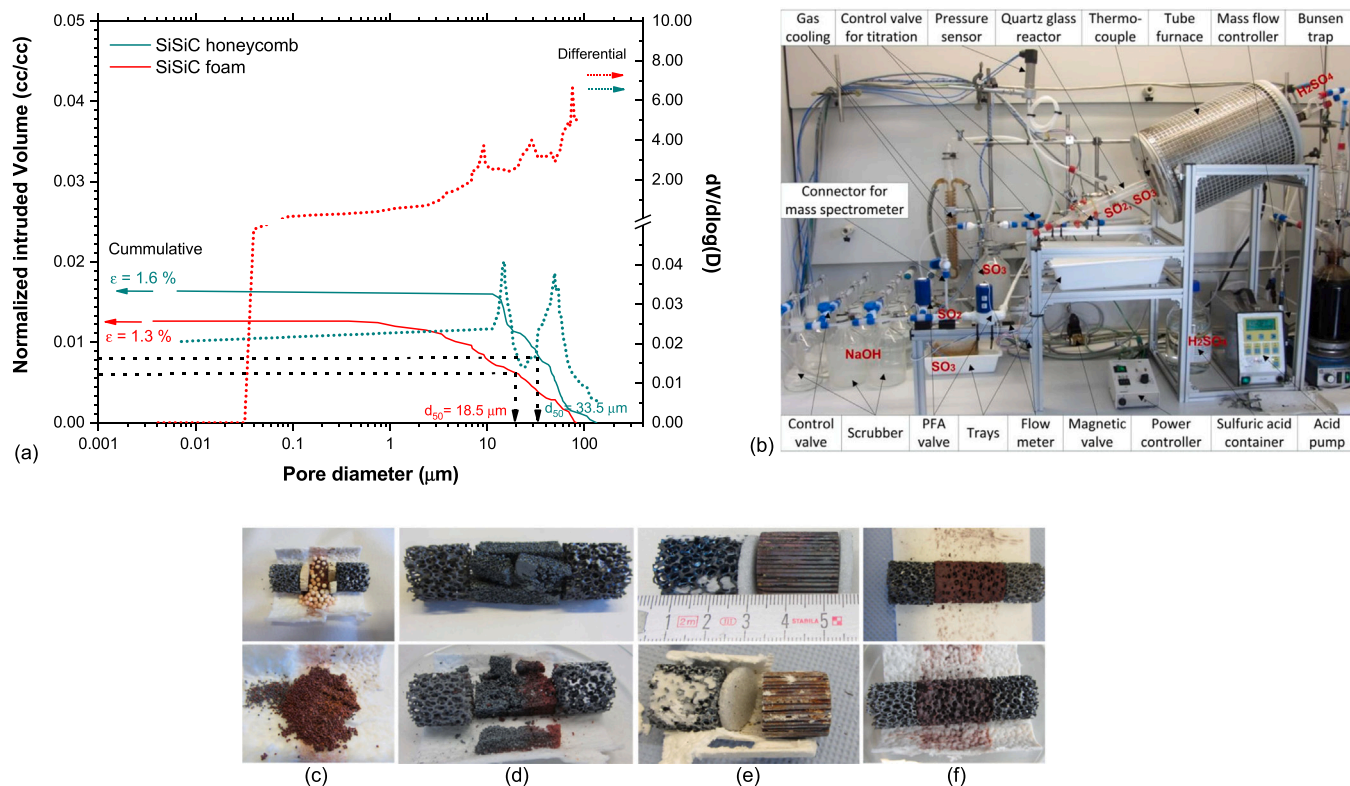


**Fig. 3.** (a) Hg porosimetry curves (cumulative and differential) of typical non-coated SiSiC honeycombs and foams employed as catalytic supports (shown in Fig. 3e, f below) from where their porosity and mean pore diameter can be determined; (b) prolonged SAD-STS test rig at DLR with furnace, quartz reactor and peripherals; (c)-(f) typical catalytic beds used therein (between non-coated SiC foams operating as flow distributors): (c) Fe<sub>2</sub>O<sub>3</sub> particles after on stream exposure in the diluted with alumina spheres catalytic cascade (top) and separated (bottom); (d)-(f) specimens before (top) and after (bottom) on-stream exposure: (d) Fe<sub>2</sub>O<sub>3</sub>-made foams; (e) Fe<sub>2</sub>O<sub>3</sub>-coated SiSiC honeycomb; (f) Fe<sub>2</sub>O<sub>3</sub>-coated SiSiC foam.

rate of liquid sulphuric acid: 0.10, 0.25 and 0.50 ml/min. Nitrogen was employed as carrier gas, its flow rate adjusted in conjunction with that of sulphuric acid so that to maintain the same  $\text{SO}_3$  mole fraction, 0.205, constant in all experiments. First the density of the concentrated liquid  $\text{H}_2\text{SO}_4$  reactant, necessary to define exactly the degree of concentration, is measured by weighing and measuring the volume ( $\sim 50$  ml) of a quantity of it. The feed rate of liquid  $\text{H}_2\text{SO}_4$  into the reactor is measured before the catalytic experiments as follows: liquid sulphuric acid is driven through a peristaltic pump (FinkChem & Tech, Model R-05-3, Dürheim, Germany) to a graduated cylinder for 30 min. Then, the volume and weight of this quantity of  $\text{H}_2\text{SO}_4$  delivered in 30 min are measured to determine the liquid  $\text{H}_2\text{SO}_4$  mass flow rate and the density again. The density used in the calculations is the average of the two density measurements above. The flow rate of the carrier Nitrogen gas is measured with the aid of a mass flow controller (MKS Instruments, Germany) pre-calibrated with a BiOs International Corporation (Model 220-L, U.S.A., accuracy of  $\pm 1\%$ ) calibration device. The temperature of the sample is measured by a K-type thermocouple with its tip reaching the end of the catalyst bed [17], while a sensor connected to the cold zone of the reactor detects the pressure inside the quartz glass reactor that is of 30 mm external and 26 mm internal diameter.

Changes of both the catalyst weight and the sulphuric acid flow rate are reflected in the Weight Hourly Space Velocity (WHSV, in  $\text{h}^{-1}$ ), which is independent of temperature and defined as the ratio of the effective inlet  $\text{H}_2\text{SO}_4$  liquid mass flow rate (in g  $\text{H}_2\text{SO}_4/\text{h}$ ) to the mass of catalyst (in g) as exactly in one of our previous relevant works [48].

The first tests performed involved screening of various PGM- and oxide-based catalytic compositions reported as state-of-the-art in the literature or having been identified to exhibit substantial catalytic activity in our previous studies [32,50]; these experiments were targeted on assessing the “robustness” of the catalytic systems and therefore were performed under the highest sulphuric acid flow rate spanned, 0.50 ml/min, and for long on-stream exposure times. This set of experiments was materialized with the catalytic materials coated on SiC honeycombs, following our previous work that involved testing of such oxide-catalyst-coated structures up to 100 h [32] and complementing it on the one hand with tests of PGM-based catalysts up to these on-stream exposure time levels and on the other hand with testing of the oxide-based ones under much longer times, reaching almost 1000 h. The catalyst compositions, loading and respective test conditions for the honeycombs are shown in Table 2. The honeycombs containing Pt-based catalyst compositions were prepared by an industrial supplier under a proprietary protocol. It should be noted that, as can be seen from the values in Table 2, the amount of active catalyst (Pt) per weight of the catalytic support oxide of the washcoat (0.8 % Pt/ $\text{Al}_2\text{O}_3$  and 1.0 % Pt/ $\text{TiO}_2$  respectively) was selected to be similar or even slightly higher than those of similar systems reported in the literature [5,26]. These catalytic systems were tested at a temperature of 650 °C vs. that of 850 °C of the oxide-based ones with the rationale that their higher cost of the former group should be counterbalanced by a superior property like e.g. similar catalytic activity at substantially lower operation temperature. The testing temperature of 850 °C for the oxide catalysts was selected based on the fact that the maximum temperature of the particles in a centrifugal receiver achieved so far is of the order of 950 °C. Parametric experiments with similar, but not identical and thus not included here, catalytic mixed oxide particles (to be reported in a future

publication) showed low  $\text{SO}_3$  conversion improvement for reaction temperature  $> 850$  °C with this improvement becoming negligible for  $> 875$  °C. On the other hand, lowering the temperature to 800 °C resulted in a profound negative effect as measured  $\text{SO}_3$  conversion at that temperature was determined to be more than 35 % lower than that at 850 °C. Hence, a reaction temperature of 850 °C was considered as optimal, allowing a “margin” of 100 °C reduction in temperature due to heat losses from the solar receiver to an allothermally-heated reactor, being suitable in parallel for nuclear VHTRs that provide Helium at the same temperature range of the order of 950 °C.

Prior to the catalytic experiments, temperature measurements at several points along the “central” area of the tubular furnace were performed under varying nitrogen gas flows by moving an adjustable thermocouple, to ensure that the temperature there was constant in a zone longer than the longest catalytic bed tested. There were no provisions for multiple temperature measurements along the reactor during the catalytic experiments; a single extra thermocouple inside a glass capillary (in addition to the one embedded in the furnace from the manufacturer to control its temperature) was used to measure the temperature at the exit of the catalytic part of the bed penetrating through a hole in the SiC foam used as a flow distributor just downstream (as illustrated in our previous relevant publication [17]); the power of the furnace was accordingly adjusted to ensure that the temperature indicated by this extra thermocouple was always the targeted one.

Structures made entirely out of iron oxide were also in-house prepared and comparatively tested: iron oxide spherical particles and iron oxide-made foams. The particles were prepared by CERTH via rotation of controllably wetted powder in a planetary mill (Fritsch Pulverisette 6) at 600 rpm without grinding media and eventual sintering under air flow at 950 °C [44]. Their diameters typically ranged from 850 to  $< 2000$   $\mu\text{m}$  with an average diameter of  $\sim 1$  mm. Their bulk density was  $\sim 2$  g/ml, their BET specific surface area 1.44  $\text{m}^2/\text{g}$  and Hg porosimetry (Micromeritics, AutoPore IV 9500 porosimeter instrument) of calcined particles resulted in non-measurable total porosity values (i.e. the particles are essentially non-porous). For the catalytic experiments the particles' bed was mixed with coarser alumina spheres (diameter range 3.5–4.5 mm - Fig. 3b) that serve a multi-fold purpose: they result in higher bed porosity and tortuosity reducing pressure drop and enhancing gas-catalyst contact and alleviate sintering between the much finer catalytic particles [17]. The foams were prepared by DLR via impregnation of polyurethane (PU) sacrificial template foams in hematite slurries and subsequent slow drying and calcination at 1350 °C in order to decompose the PU foam and form a sintered iron oxide one [46]. Typical such structures are shown in Fig. 3c, d. All iron oxide-containing specimens and the respective catalysts' weight, dimensions and bulk densities of the catalytic beds are listed in Table 3. In several cases, mentioned explicitly in the discussion below, these parametric tests were performed with the same specimen inside the tube furnace in order to assess in parallel its stability and endurance after prolonged on-stream exposure. As in previous studies [17,32] the conversion of  $\text{SO}_3$  to  $\text{SO}_2$  was measured by two complementary techniques: (a) by trapping of  $\text{SO}_2$  in a Bunsen trap followed by titration of the remaining  $\text{I}_2$  with sodium- thiosulfate and (b) by employing an oxygen sensor to in-situ measure the  $\text{O}_2$  concentration in the gaseous effluent stream which is directly correlated to the  $\text{SO}_3$  conversion via the

**Table 2**  
Catalyst-coated SiSiC honeycombs employed in long-term catalytic testing: characteristics and testing conditions.

Catalyst	Honeycomb mass before coating (g)	Honeycomb mass after coating (g)	Loading (wt %)	Loading (g)	Catalyst amount (g)	Temperature (°C)	Time on stream (h)
Pt on $\text{Al}_2\text{O}_3$	14.08	16.53	17.4	2.45	Pt: 0.02	650	100
Pt on $\text{TiO}_2$	16.90	19.77	17.0	2.87	Pt: 0.03	650	105
$\text{Fe}_2\text{O}_3$	11.04	12.74	15.4	1.70	$\text{Fe}_2\text{O}_3$ : 1.70	850	547
$\text{Fe}_{0.7}\text{Cr}_{1.3}\text{O}_3$	12.09	14.12	16.8	2.03	$\text{Fe}_{0.7}\text{Cr}_{1.3}\text{O}_3$ : 2.03	850	942

**Table 3**

Iron oxide-catalytic structures employed in the sulphur trioxide splitting tests, respective catalyst amount ( $\text{Fe}_2\text{O}_3$ ), dimensions and bulk densities of respective catalytic beds.

	Catalyst ( $\text{Fe}_2\text{O}_3$ ) weight (g)	Loading (wt%)	Catalytic bed total weight (g)	Catalytic bed length (cm)	Catalytic bed volume ( $\text{cm}^3$ )	Catalytic bed bulk density ( $\text{g}/\text{cm}^3$ )	Time on stream (h)
$\text{Fe}_2\text{O}_3$ -coated honeycomb	1.83	17.6	12.23	2.54	11.83	1.04	100
$\text{Fe}_2\text{O}_3$ -coated honeycomb	1.70	15.4	12.74	2.54	11.83	1.08	547
$\text{Fe}_2\text{O}_3$ -coated foam	4.32	41.2	14.83	4.00	20.27	0.73	362
$\text{Fe}_2\text{O}_3$ -made particles (with alumina spheres)	8.00	–	$8.00 + 12 = 20$	2.46	12.47	1.60	118
$\text{Fe}_2\text{O}_3$ -made particles measured separately						2.00	
$\text{Fe}_2\text{O}_3$ -made foams	13.22	–	13.22	3.00	15.20	0.87	609

stoichiometry of reaction (1b) (Table 1). The reader is referred to our previous recent work [17] for an extensive discussion on the accuracy and complementarity of these two techniques.

The catalytic structures were comparatively characterised before and after exposure to reaction conditions (denoted as “fresh” and “used” states, – Fig. 3c-f, top, bottom, respectively); the characterisations involved phase composition by X-Ray Diffraction/XRD (Siemens D-500 Kristalloflex X-ray diffractometer, Cu  $K\alpha$  radiation), and microstructure and elemental composition by Scanning Electron Microscopy/SEM (DLR: ZEISS ULTRA 55 FEG, Karl Zeiss, Oberkochen, Germany, instrument coupled with an INCA Pentafet x3 Electron Dispersive Spectroscopy/EDS X-ray microanalysis system, Oxford Instruments; CETH: JEOL 6300 microscope coupled with a Link ISIS 300, Oxford Instruments, EDS X-ray microanalysis system) and with Inductively Coupled Plasma Atomic Emission Spectroscopy/ICP-AES (Optima 4300 DV, Perkin Elmer). For the SEM analysis the iron-oxide-based samples were fixed on adhesive carbon tapes and conductivity was provided through Pt coating by a sputter coater (BAL-TEC SCD 500). The Pt-

containing samples were coated with carbon. Possible formation of sulphates during on-stream exposure was investigated via subjecting samples of the fresh and used catalysts to ThermoGravimetric Analysis/TGA under air flow using a Netzsch STA 449 F3 Jupiter® instrument and monitoring any weight loss. The samples were heated to 1000 °C with a ramp of 5 °C/min and cooled with the maximum possible rate to room temperature; some “used” samples were subjected to a second cycle to determine whether the weight changes were actually completed during the first one.

For the evaluation of pressure drop caused by the application of the catalyst layer(s) upon the commercial ceramic foam substrates (permeability measurements), the samples were canned inside a custom-made flow-through holder. During the sample preparation, its perimeter was “sealed” with a tightly wrapped ceramic felt of very low permeability, to ensure that the applied flow, in this case air at ambient temperature, enters only through the inlet of the sample and is headed towards its outlet passing only through the samples’ channels/ pores. The system was connected with a mass flow controller (Brooks

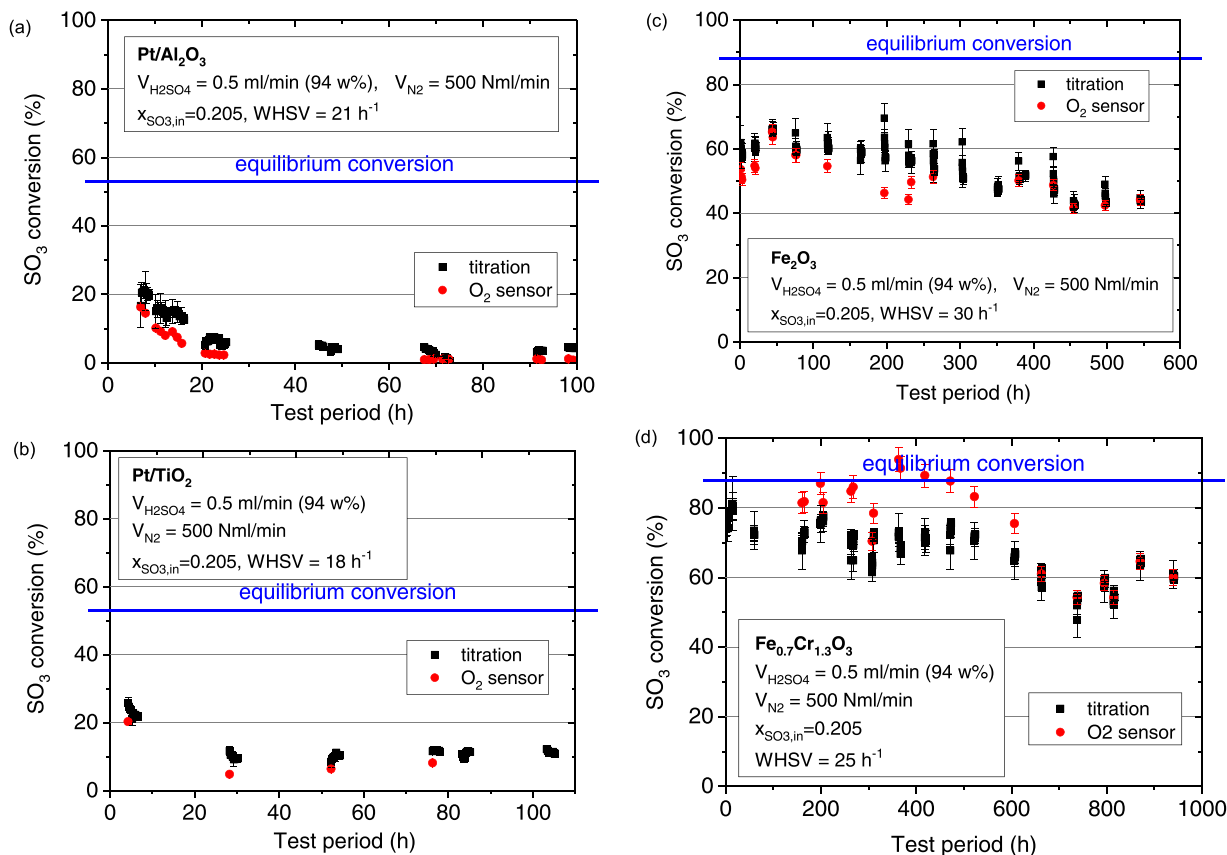


**Fig. 4.** Prolonged  $\text{SO}_3$  splitting tests of catalyst-coated SiSiC honeycombs ( $\text{SO}_3$  conversion vs. reaction time) under sulphuric acid flow rate 0.5 ml/min: (a) Pt/ $\text{Al}_2\text{O}_3$  (650 °C); (b) Pt/ $\text{TiO}_2$  (650 °C); (c) commercial  $\text{Fe}_2\text{O}_3$  powder (850 °C); (d) in-house synthesized  $\text{Fe}_{0.7}\text{Cr}_{1.3}\text{O}_3$  (850 °C).

Instrument BV), calibrated for air, and a pressure transmitter (JUMO dTRANS p02) able to measure in-line the pressure difference between the air flow inlet and outlet. During the procedure the air flow is increased stepwise from 0 to 100 l/min (std) in 5 l/min steps and for each flow the pressure is simultaneously measured at the inlet and the outlet of the segment leading to the recording of the pressure drop until a stable value is obtained.

### 3. Results and discussion

#### 3.1. Catalytic activity of PGM- and oxide-based catalyst-coated SiC honeycombs

The results of the first set of tests with PGM- and oxide-based catalyst-coated SiC honeycombs are shown in Fig. 4a-d. It should be noted that the values of WHSV in the case of Pt catalysts shown in the respective graph legends are calculated per the total weight of coating i. e. that of Pt plus that of the oxide catalyst carrier ( $\text{Al}_2\text{O}_3$ ,  $\text{TiO}_2$ ) shown in the 5th column of Table 2. The first conclusion is that the PGM-based catalysts demonstrated not only much lower conversion than the respective equilibrium one (at the lower testing temperature of 650 °C and  $\text{SO}_3$  partial pressure employed) but fast deactivation as well. The Fe-Cr mixed oxide demonstrated the highest conversion values, very close to the thermodynamic ones and steady for the first 550 h of the respective test. Thus, its testing period was extended to 950 h; however, deactivation was observed during this longer on-stream exposure. This deactivation can be attributed to eventual leaching of Cr, which is a phenomenon already identified in past relevant studies [51]. One of our previous relevant studies [48] has shown that during relatively short-time (45–60 min) catalytic experiments, commercial  $\text{Cr}_2\text{O}_3$  powder exhibited an observable Cr-leaching behavior in contrast to several  $\text{Fe}_{2-x}\text{Cr}_x\text{O}_3$  compositions that did not. However, the present long-term

exposure test of  $\text{Fe}_{0.7}\text{Cr}_{1.3}\text{O}_3$  (Fig. 4d) made evident that this Fe-induced stabilization of Cr actually relates with the delay of this leaching phenomenon rather than its elimination. The “plain” iron oxide exhibited high conversion values, in the range of 60–70 %, much higher than these of the Pt-based ones, yet somewhat lower than those of the mixed oxides and also a gradual decrease of conversion as the time on stream exceeded 250 h. Conversion eventually stabilized to levels of ~ 40 % with longer on-stream exposure times.

The respective comparative phase composition (XRD) diagrams are shown in Fig. 5a-d. For this analysis, the spectra of the “fresh” catalysts were obtained with samples of the catalysts in their powder form, whereas for the “used” catalysts, samples were taken from both the inlet and the outlet of each catalyst-coated honeycomb tested. Since it was not possible to isolate the catalyst coating from the support, all such “used” samples (except 5b) contain a significant amount of the SiSiC support phase and hence the XRD spectrum of this support is also provided for reference. From the comparison becomes evident that on the one hand, in all cases the phase compositions at the reactor’s inlet and exit are practically identical. On the other hand, both oxide catalysts do not show any appreciable phase composition differences before and after their long-term on-stream exposure. On the contrary, the Pt-containing catalysts exhibit significant alterations before and after reaction, with the most prominent being that of the Pt/ $\text{Al}_2\text{O}_3$  one where extensive sulphation can be observed manifested via distinct peaks corresponding to a crystalline  $\text{Al}_2(\text{SO}_4)_3$  phase over an “amorphous-like” background (the latter being characteristic for both Pt-containing catalysts). This extensive sulphation is most likely the cause of this catalyst’s rapid deactivation, since, even though due to its small quantity, the metallic catalyst phase cannot be detected via XRD. Elemental analysis via EDS corroborated the existence of Pt on the exposed catalysts. However, a measurable decrease in Pt content was identified via ICP measurements in the exposed samples as compared to the fresh ones.

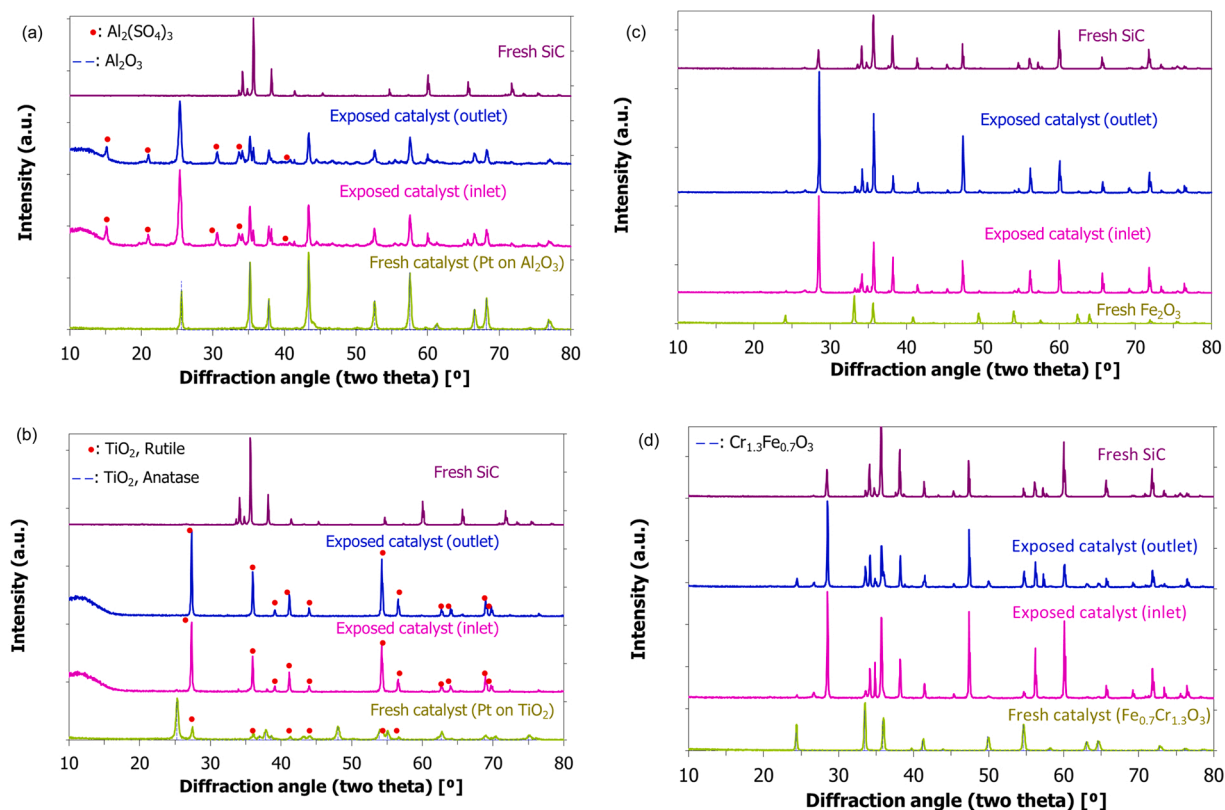


Fig. 5. Comparative phase composition analyses (XRD spectra) of catalyst-coated SiSiC honeycombs before and after their on-stream exposure (the spectrum of the SiSiC support is provided for reference, since the catalytic samples contain a significant amount of it) (a) Pt/ $\text{Al}_2\text{O}_3$ ; (b) Pt/ $\text{TiO}_2$ ; (c) commercial  $\text{Fe}_2\text{O}_3$  powder; (d) in-house synthesized  $\text{Fe}_{0.7}\text{Cr}_{1.3}\text{O}_3$ .

This could be attributed to limited Pt sublimation phenomena known to occur at high temperature and/or leaching effects reported in some studies [52]. Furthermore, the use of Pt-catalyst carriers like alumina and titania in the present study, mitigates any direct interactions between the Pt active catalysts and the oxygen evolved during  $\text{SO}_3$  splitting with the SiSiC porous support, as observed in several studies that employed Pt directly supported on SiC [53,54]. In such previous studies the XRD spectra of the used catalysts are characterized by a blunt peak at about  $22^\circ$  corresponding to  $\text{SiO}_2$  formed in-situ due to oxidation of the SiC support from the  $\text{O}_2$  evolved. In our case where SiSiC is employed as support, free Si on the surface is expected to be oxidized to  $\text{SiO}_2$ , a phenomenon already confirmed in our previous collaborative work, especially when employing non-coated SiSiC honeycomb supports to evaluate their own “blank” catalytic activity [50]. However, as can be observed in the XRD graphs of Fig. 5, there is no sign of either such  $\text{SiO}_2$  formation or of any SiOC phases in any of the catalytic systems used, either Pt- or iron oxide-based ones. In all cases, the coating load – and thus coverage of the surface of the support structure, is already substantial and oxidation is expected to be limited due to limited direct support-oxygen contact. Most likely this explains the absence of SiOx phases in the XRD patterns of both fresh and used catalytic structures. In any case, the existence of such carrier-related sulphates cannot be unambiguously corroborated by XRD alone, unless their content exceeds a minimum traceable concentration (like in the case of Pt/ $\text{Al}_2\text{O}_3$ ); thus, TGA experiments were performed on the exposed samples (reported in a subsequent section, in comparison to the iron-oxide catalyst ones).

### 3.2. Catalytic activity of iron oxide structured systems

Based on the above results and with the eventual target of building a scaled-up, proof-of-concept allothermally heated reactor (Fig. 2), it was decided to employ iron oxide as the catalytic material of choice. The argumentation in favour of this approach is that iron oxide is commercially available in large quantities and inexpensive, and the difference in conversion between this and the mixed Fe-Cr oxide is counterbalanced by the avoidance of the large-scale synthesis step for the mixed oxide. Yet, to increase the conversion of iron oxide, approaches like employing a lower sulphuric acid flow rate and/or increasing the quantity of the active iron oxide catalyst in the reactor volume can be adopted. Indeed, Fig. 6 shows the performance of another  $\text{Fe}_2\text{O}_3$ -coated SiSiC honeycomb under the lowest sulphuric acid flow rate tested, 0.10 ml/min, for 100 h, compared to that of the non-coated honeycomb, reported in previous studies [32,50]. At this lower flow rate, conversion of the former reached a stable value very close to the equilibrium value of 88 %

corresponding to the specific temperature. As already reported in the aforementioned previous studies, the latter, uncoated SiSiC honeycomb, exhibits also non-negligible yet low  $\text{SO}_3$  conversion, due to non-catalytic, thermal-only  $\text{SO}_3$  splitting enhanced by catalytically active iron impurities.

Furthermore, to increase the catalyst mass in the reactor volume, on the one hand higher loadings, of the order of ca. 35 – 40 wt % were targeted in the next series of  $\text{Fe}_2\text{O}_3$ -coated supports prepared, namely the SiSiC foams, and on the other hand structures entirely made out of iron oxide were manufactured; namely particles and foams.

The  $\text{SO}_3$  conversion (as measured by titration) results of the experiments with a  $\text{Fe}_2\text{O}_3$ -coated foam of 41 wt% loading, are shown in Fig. 7. The experiments were performed with the same specimen, accumulating hence a total of 362 h on-stream. Following the course of the experiment from “left-to-right”, the particular specimen exhibited very high conversion at 850 °C even at the highest sulphuric acid flow rate, which with decreasing flow rate, reached the equilibrium level. This finding shifted the next test experiment to lower rather than higher temperature levels (800 °C), where, like in all cases, increasing the sulphuric acid flow rate resulted to lower conversion. Repetition of the cycle test with the three different flow rates at 850 °C, demonstrated full reproducibility of near-equilibrium conversion. It is worth mentioning that these values are in the same range, yet slightly higher, with those of the  $\text{Fe}_2\text{O}_3$ -coated honeycomb under the same temperature and sulphuric acid flow rate conditions shown in Fig. 6 and stable for a longer time period. Thus, the  $\text{Fe}_2\text{O}_3$ -coated foams seem to be very active and very robust systems as well and in principle, most promising for their incorporation in the allothermal reactor.

In general, cellular ceramics like honeycombs and foams provide one of the most effective ways of packing a lot of geometric surface area into a small volume and with their very high open frontal area ensure a much lower pressure drop than the packed beds of spherical particles or porous catalysts pellets [24]; this small pressure drop is only marginally augmented by the thin catalyst/washcoat layers even at high loadings [55] as also shown in Section 3.4 below. Ceramic foams in particular are characterized by their extremely high, yet interconnected, porosity that provides for a very low pressure drop and enhanced mass and heat transfer due to high convection in the tortuous megapores [56]. Indeed the void fraction of the honeycombs used herein calculated as their open frontal area from the dimensions of their flow-through channels occurred  $\approx 46\%$  whereas the void fraction of the foams  $\approx 76\%$  [57]. Furthermore, due to their very high available area, can accommodate relatively high amounts of the catalytically active phase and at the same

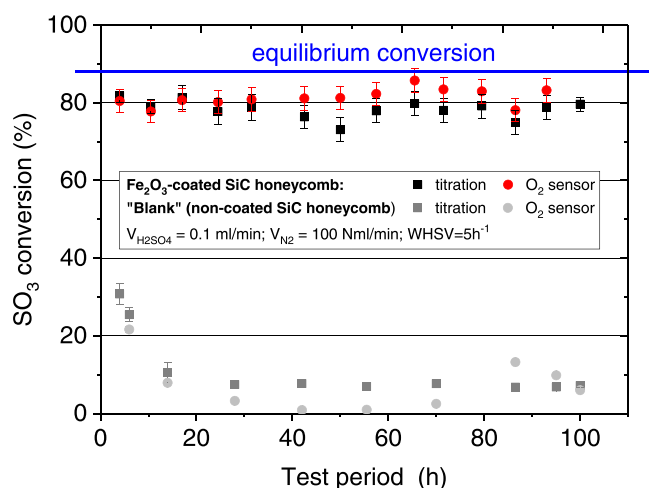


Fig. 6.  $\text{SO}_3$  splitting test of  $\text{Fe}_2\text{O}_3$ -coated SiSiC honeycomb with the lowest sulphuric acid flow rate tested, 0.10 ml/min at 850°C, compared to a “blank” experiment (non-coated SiSiC honeycomb) under the same conditions.

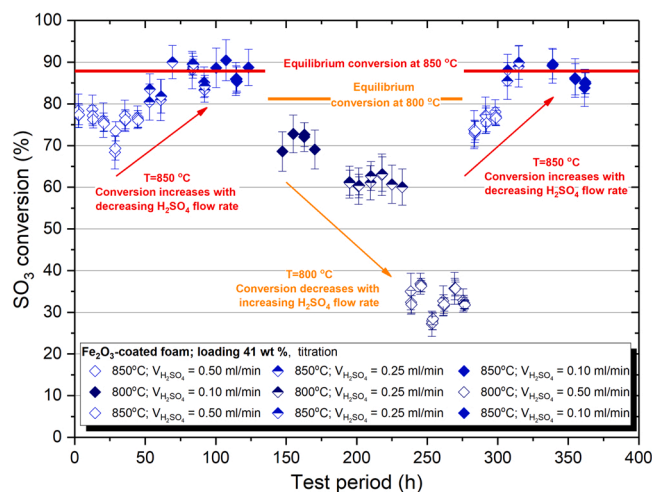


Fig. 7. Prolonged  $\text{SO}_3$  splitting testing of  $\text{Fe}_2\text{O}_3$ -coated SiSiC foam:  $\text{SO}_3$  conversion vs. reaction time as a function of reaction temperature (850, 800 and again 850 °C) and sulphuric acid flow rate (0.10, 0.25 and 0.50 ml/min).

time keep it in adequately high dispersion within the structured reactor's volume thereby mitigating undesired sintering effects. Last but not least, compared to flow-through honeycombs, foams exhibit a considerable degree of radial mixing, advantageous in heat transfer-limited processes like the ones under study in this work. Heat transfer is further enhanced by the high thermal conductivity of the support material, SiSiC (for dense materials it is  $\approx 100$  W/m·K vs.  $\approx 1$  W/m·K of cordierite for example). Despite the expected fact that the effective conductivity of highly porous structures like the ones employed here is much lower, measurements on such SiSiC foams have shown that it ranges between 1 and 5 W/m·K and in fact increases with increasing temperature, and naturally, with increasing ppi number, mainly due to the larger heat transfer surface for the materials with smaller cells [57, 58].

The experiment with the particles was performed by varying the operating conditions with the same particles batch in the furnace, which, hence, remained for a total of 120 h on-stream. As already mentioned, in the specific experiments the particles' bed was mixed with coarser alumina spheres (Fig. 3c). The results are shown in Fig. 8a. In accordance to previous shorter-term tests [44] the particles exhibited an initial conversion of around 45 % at the higher flow rate, which though, decreased to subsequently stabilize in the range 25–30 % with increasing time on stream. Lowering the sulphuric acid flow rate raised the conversion to levels between 55 % and 65 %. However, in the process of performing consecutively a second cycle under the initial higher flow rate and in order to verify the reproducibility of the results, conversion dropped significantly to much lower levels than those achieved during the first cycle; this result was construed as an indication of catalytic activity's deterioration with prolonged time on-stream and hence the experiment was not continued further.

A similar trend was observed with the  $\text{Fe}_2\text{O}_3$ -made foams. Fig. 8b shows the results of this set of parametric experiments, that were performed with the same sample inside the reactor, having thus accumulated a total of 609 h on-stream exposure. Three sulphuric acid flow rates 0.10, 0.25 and 0.50 ml/min were tested at three temperature levels, 850, 900 and 950 °C. At the beginning of the experiment and at 850 °C under the highest sulphuric acid flow rate, the foams exhibited an initial conversion of  $\sim 50$  % which, however, similarly to that of the  $\text{Fe}_2\text{O}_3$ -made particles (Fig. 8a), dropped dramatically to stabilize after 70 hrs on-stream in the range of  $\sim 10$ –15 %, lower than those of all other systems under the same conditions. Decreasing the sulphuric acid flow rate increased the conversion, even though a temporary malfunction in the iodometry titration measurement setup identified after the experiment with 0.10 ml/min sulphuric acid flow rate lead to very high error

margins and thus the specific results are not plotted. Thus, the experiments were shifted to higher reaction temperatures 900 and 950 °C (following the course from “left-to-right” in Fig. 8b), but only at 950 °C and for the lowest flow rate tested (0.10 ml/min) conversion exceeded 70 %. An interesting observation is their colour change from grey to red near the entrance of the bed. The rather low activity of the particular foam structures - lower than that of the iron oxide particles under the same reaction conditions (“red” points in Fig. 8a, b respectively) - is most likely attributed to the very high calcination temperature (i.e. 1350 °C) employed for their preparation, which was necessary in order to obtain mechanically stable foam structures. Evidently, such high treatment temperature resulted to profound sintering of iron oxide grains that affected adversely their catalytic activity.

### 3.3. Post reaction characterisation of catalytic systems

#### 3.3.1. Thermogravimetric analysis (TGA)

The relevant weight change curves of the “used” catalyst structures are shown in Fig. 9; to facilitate comparisons the curves are grouped in different graphs on different weight-axis scales. The weight losses marked with arrows in the graphs correspond to those taking place in the higher-temperature range, attributed to the respective metal sulphates' dissociation at specific temperatures, based on similar, previously reported experiments with commercial sulphate powders [48] and not to the overall weight loss from the beginning of the TGA experiment. For an “objective” comparison, the weight loss in the cases of coated specimens has been calculated both per the entire weight of the structured sample as well as per the amount of catalyst coated on it, given their known catalyst loadings and percentages, as provided in Tables 2 and 3.

In Fig. 9a the curves for the two Pt-catalyst coated samples are shown, as measured with catalyst coating “scratched” away from the support. The extremely high weight loss ( $\sim 35$  %) of the Pt/ $\text{Al}_2\text{O}_3$  sample should be noted; the deactivation of the particular catalyst can be attributed to this extensive sulphates' formation. The weight loss of the Pt/ $\text{TiO}_2$  catalyst is much lower,  $\sim 1.6$  %. Fig. 9b shows the relevant curves of the  $\text{Fe}_2\text{O}_3$ - and  $\text{Fe}_{0.7}\text{Cr}_{1.3}\text{O}_3$ -catalyst-coated SiSiC honeycombs tested for 547 and 942 hrs respectively. These tests were performed with ground pieces sectioned from the coated specimens, including the support; thus, the weight loss can also be calculated with respect to the initial catalytic coating weight only (to be compared to those of the Pt-based systems at least qualitatively), given the known catalyst loading (and considering the TGA sample representative of the whole coated structure). In both cases, weight losses of these two catalytic systems are

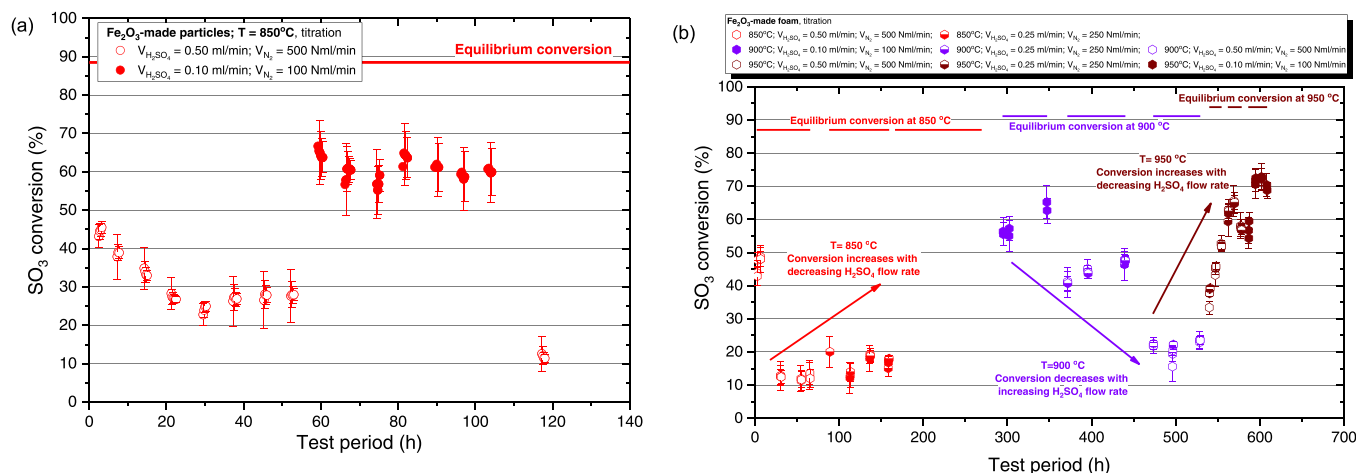


**Fig. 8.** Prolonged  $\text{SO}_3$  splitting testing of (a)  $\text{Fe}_2\text{O}_3$ -made particles, at 850 °C:  $\text{SO}_3$  conversion vs. reaction time as a function of sulphuric acid flow rate (0.10 and 0.50 ml/min); (b)  $\text{Fe}_2\text{O}_3$ -made foams:  $\text{SO}_3$  conversion vs. reaction time as a function of reaction temperature (850, 900 and 950 °C) and sulphuric acid flow rate (0.10, 0.25 and 0.50 ml/min).

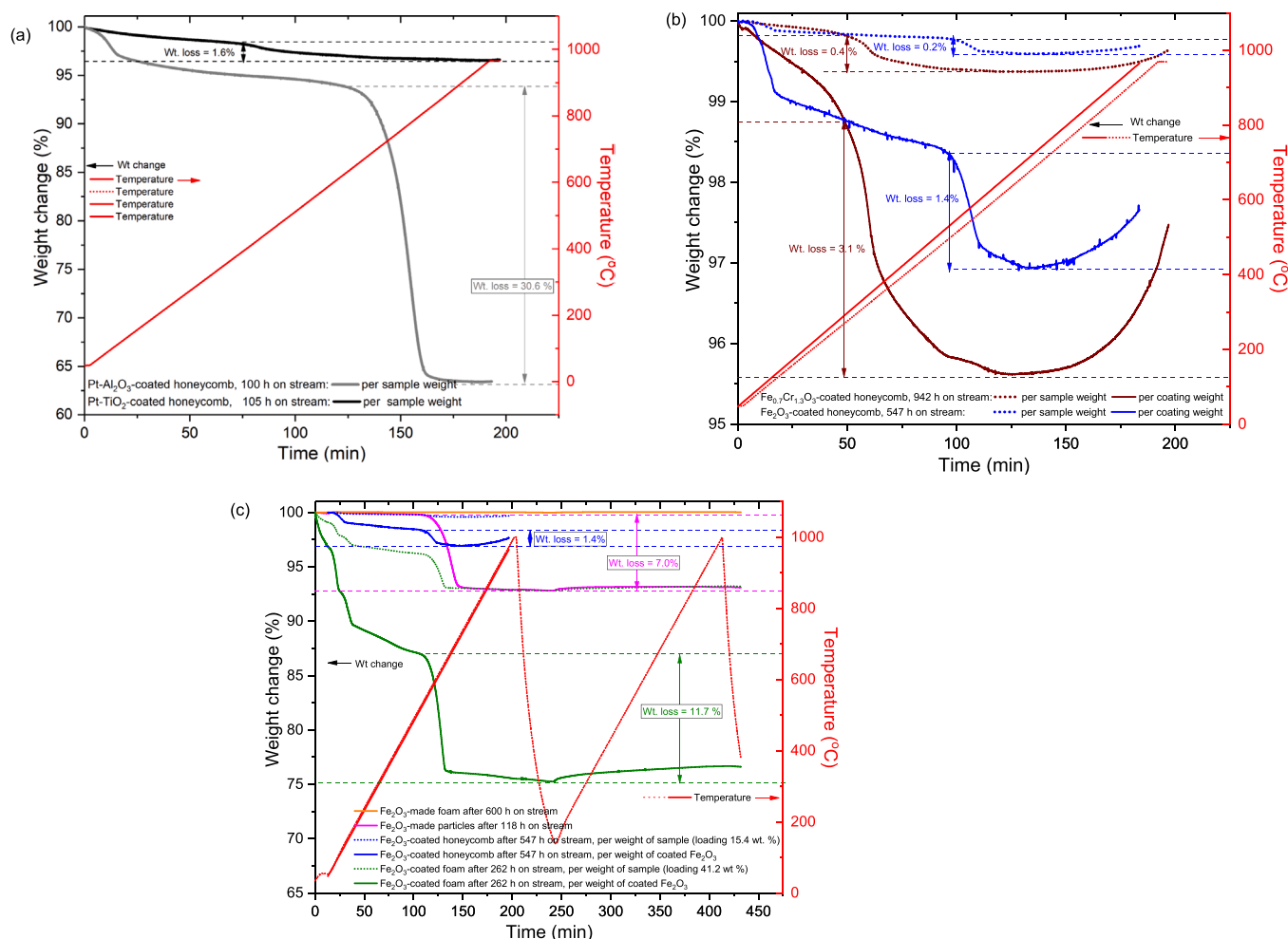


**Fig. 9.** Post-reaction TGA under air of “used” catalytic structures indicating weight loss attributable to metal sulphates’ dissociation (note the different y-axis scales in the three graphs): (a) Pt-based catalyst-coated SiSiC honeycombs; (b) Fe<sub>2</sub>O<sub>3</sub> and Fe<sub>0.7</sub>Cr<sub>1.3</sub>O<sub>3</sub> catalyst-coated SiSiC honeycombs tested for 547 and 942 hrs respectively, (c) comparison among Fe<sub>2</sub>O<sub>3</sub>-only-based catalytic structures.

much lower, despite their much longer testing time.

In Fig. 9c, the respective TGA curves of all the iron oxide catalytic structures are shown: two made entirely of Fe<sub>2</sub>O<sub>3</sub>, particles and foams, and of a Fe<sub>2</sub>O<sub>3</sub>-coated SiSiC honeycomb and a SiSiC foam. All samples except the Fe<sub>2</sub>O<sub>3</sub>-made foam, exhibit significant weight loss attributed to the respective iron sulphates formed, in exact analogy with previous TGA experiments on honeycombs coated with iron- and copper-oxide catalytic systems but tested with respect to their catalytic activity for only one hour on stream [48]. The appearance of such weight loss in all “used” catalyst specimens can be construed as a qualitative corroboration of formation of sulphates as intermediate products. On the other hand, this weight loss cannot be directly quantitatively correlated to “comparative catalyst performance”. As discussed in previous works, any weight loss associated with the dissociation of residual sulphates, depends strongly on the reactor’s cooling protocol adopted in any particular set of experiments with respect to the relevant atmosphere selected at the catalytic experiments’ completion that can “freeze” to a different degree the amount of any metal sulphates formed. Furthermore, in the case of coated samples the much lower size of the sample sectioned for TGA, might be not representative of the structures’ overall loading with catalyst, affecting thus the value of the weight loss measured.

### 3.3.2. Scanning electron microscopy (SEM) - energy dispersive X-ray spectroscopy (EDS)

Possible reaction mechanisms and differences among the catalytic

formulations tested were further elucidated via SEM/EDS analysis. Fig. 10 shows typical SEM photographs of the Pt-TiO<sub>2</sub> catalytic system, before and after exposure under reaction conditions. In the latter case samples from both the inlet and the outlet of the catalytic structure were taken to investigate any differences. From the three sets of SEM photographs (under the same magnification to better illustrate different or common features) significant microstructural differences before and after reaction or between the inlet and outlet are not distinguishable. Mapping images (Fig. 10c) show uniform distribution of coating & good uniformity of Pt dispersion in the coating in the catalyst’s pristine state. From Fig. 10d can be inferred that the coating is of uniform thickness along the full length of the honeycomb channels even after on-stream exposure. Elemental mapping analysis (Fig. 10g, j) shows clearly the sulphur collocated with Ti on the spent catalysts; sulphur’ presence is more intense near the entrance and hardly detectable near the exit. In addition, the lower intensity of Pt in the same samples, in qualitative agreement with the ICP results, suggests a decrease of the Pt concentration after reaction, due to possible leaching.

Analogous SEM photographs and analysis for the Pt-Al<sub>2</sub>O<sub>3</sub> system before and after on-stream exposure are shown in Fig. 11. Fig. 11a demonstrates uniform coating distribution along the channel of the fresh catalyst whereas relevant elemental mapping photographs of Fig. 11b show uniform distribution of coating and good uniformity of Pt dispersion within it. Fig. 11c of the spent catalyst demonstrates that the coating uniformity along the entire length of the honeycomb channels is maintained even after on-stream exposure. Relevant mapping analysis

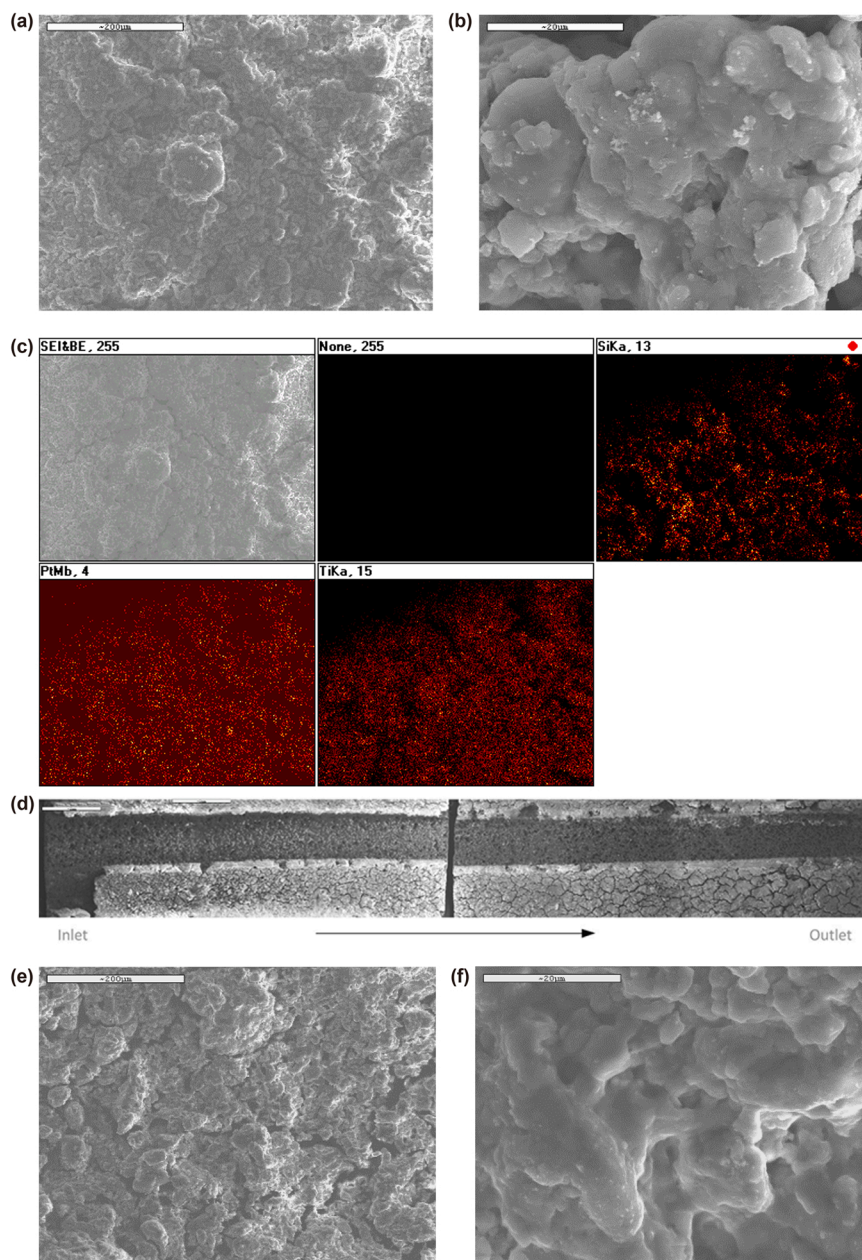


**Fig. 10.** SEM photographs under the same two magnifications and surface EDS microanalysis of the Pt-TiO<sub>2</sub>-coated SiSiC honeycomb in its pristine state (a), (b), (c) and after 105 h on-stream exposure; in the latter case photographs of the full length of a single coated channel (d) and of specimens from the inlet (e), (f), (g) and the outlet (h), (i), (j) of the honeycomb channels are shown. Presence of sulphur and reduced concentration of Pt can be qualitatively identified on the used catalyst.

(Fig. 11c) confirms that Pt remains evenly dispersed after exposure and that sulphur mapping follows the one of alumina.

Typical SEM photographs of the Fe<sub>2</sub>O<sub>3</sub>-coated SiSiC foam after 262 h on-stream exposure at small magnifications in Fig. 12a-c show the morphology of the coated foam and of the support-coating interface and provide an estimate of the catalyst coating thickness. Higher magnifications on the catalyst coating (Fig. 12d) reveal its characteristic dual-phase morphology, comprised of extensive elongated rod-like structures and much smaller quasi-spherical particles, which becomes much more distinguishable on the even higher magnifications of Fig. 13. Elemental EDS microanalysis at characteristic points showed clearly the presence of sulphur together with iron and oxygen at the elongated rod-like structures (Fig. 13a) and therefore the formation of iron sulphates and, in parallel, the lack of sulphur at the spherical particles (the minute sulphur traces recorded at these points are due to dispersion from the

neighboring sulphate formations). This becomes even clearer from the SEM/EDS analysis at an area at the center of the image of Fig. 13a containing only quasi-spherical particles and the respective EDS spectra at the two characteristic points indicated shown in Fig. 13b. This identifies their composition as iron oxide particles and SiSiC support, respectively. Again, the minor sulphur peaks are due to dispersion from the neighboring sulphates not shown on the image. The Pt and C peaks in the EDS spectra are due to the conductive coating and adhesive tapes, respectively.

SEM photographs of the same foam but after the TGA under air (see previous paragraph) are shown in Fig. 14. Fig. 14b, demonstrates clearly the absence of the elongated particles of Fig. 13a. The respective EDS spectra on other, much finer, sparse elongated structures shown in Fig. 14b, are also characterized by the complete absence of any sulphur peaks. The same conclusion occurs from the EDS on the fine, quasi-

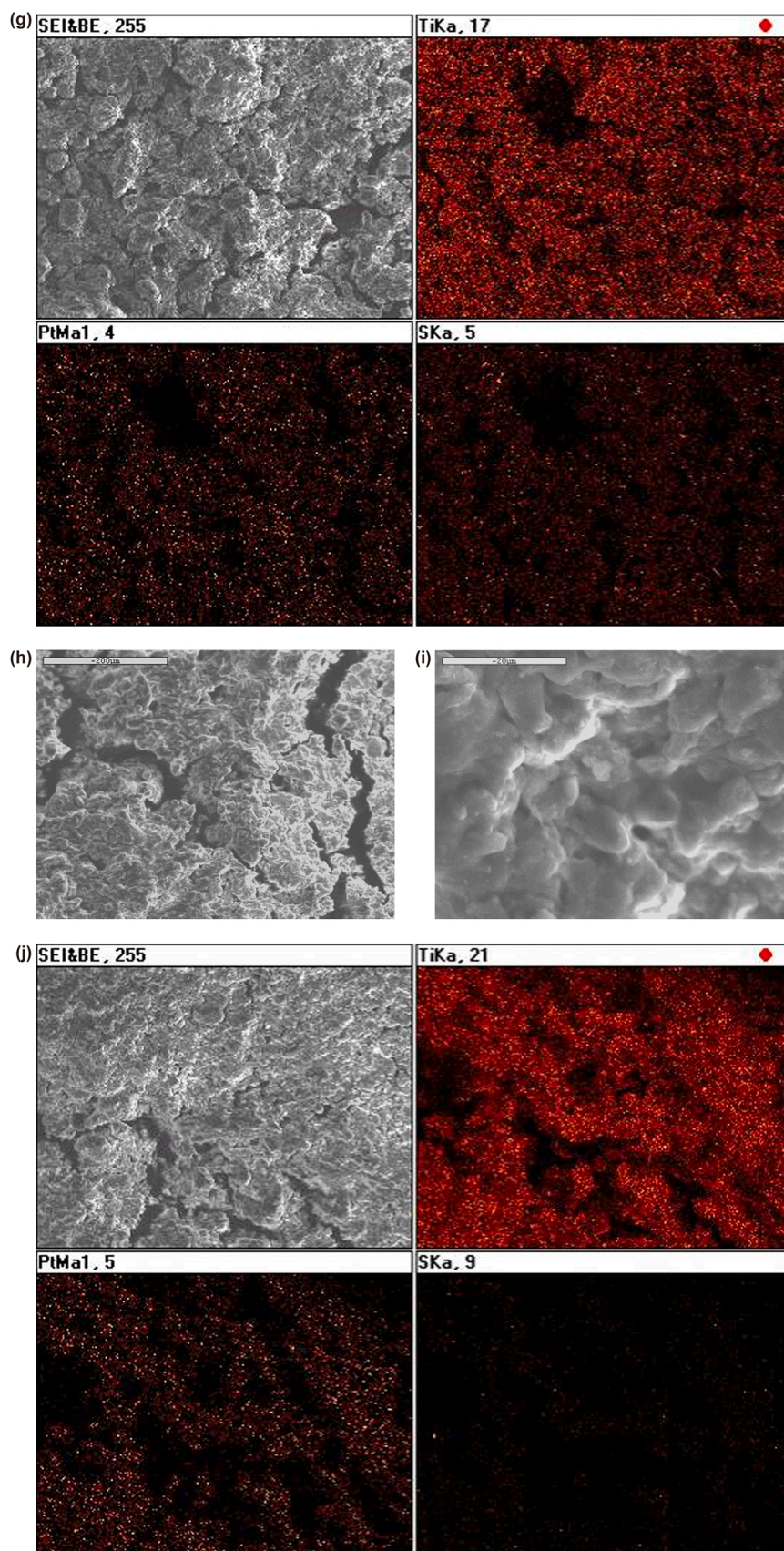
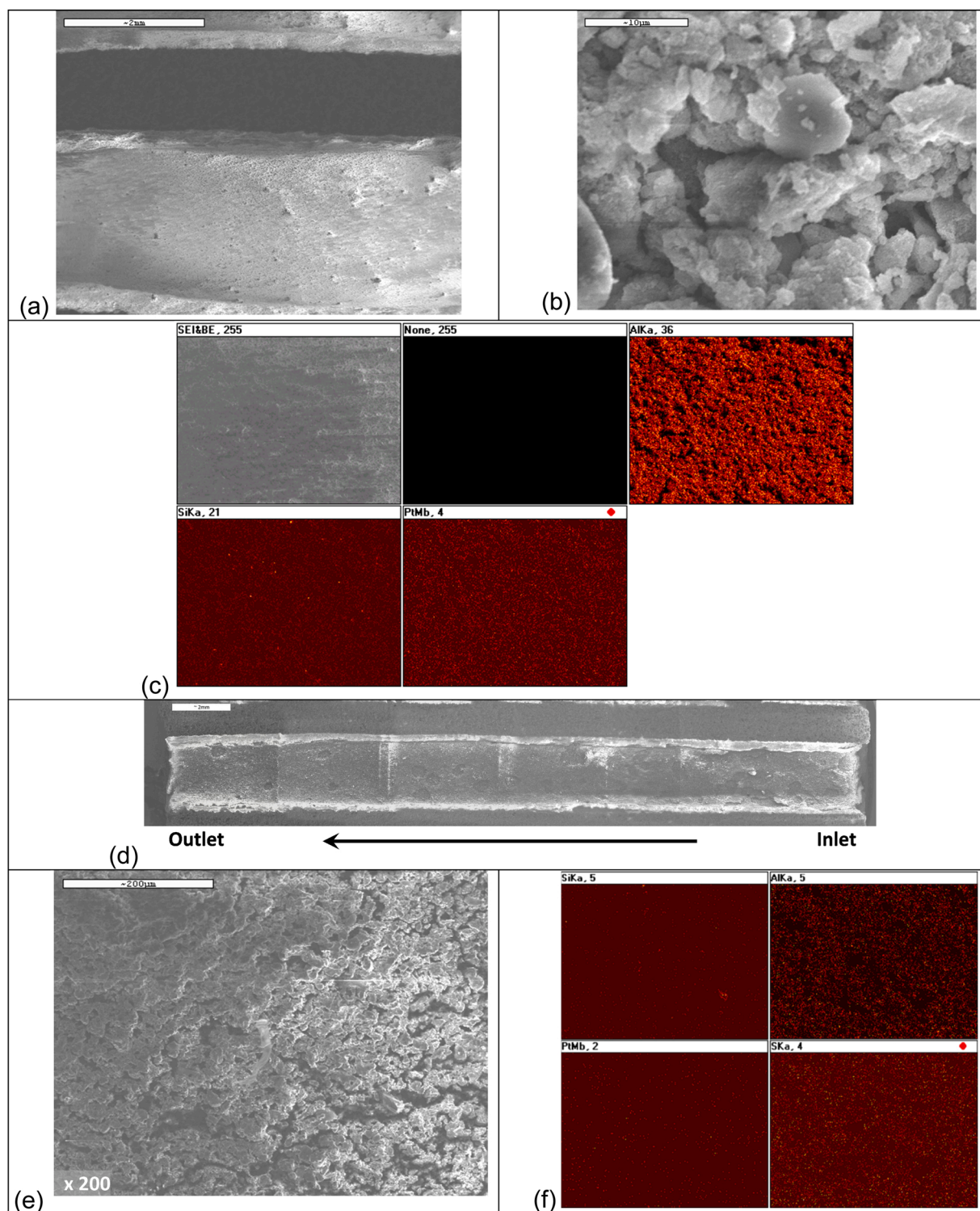


Fig. 10. (continued).

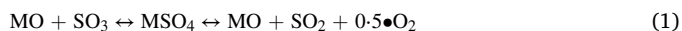


**Fig. 11.** SEM photographs and surface EDS microanalysis of the Pt-Al<sub>2</sub>O<sub>3</sub> coated SiSiC honeycomb in its pristine state (a), (b), (c) and after 100 h on-stream exposure; in the latter case photographs of the full length of a single coated channel (d) and of an area from the inlet (e), (f) are shown; presence of sulphur collocated to that of aluminum and reduced concentration of Pt can be qualitatively identified on the used catalyst.

spherical particles shown in Fig. 14c, and consisting entirely of iron oxide.

From the above it can be deduced that even for metal oxides (MO) that have lower propensity of sulphates' formation like Fe<sub>2</sub>O<sub>3</sub>, it is important to establish an optimum balance between the formation of intermediate metal sulphates (MSO<sub>4</sub>) and their dissociation to yield the reaction products, according to the following general simplified scheme

[48]:



In case SO<sub>3</sub> is fed at rates exceeding the sulphate dissociation rate into SO<sub>2</sub>, O<sub>2</sub> and the initial metal oxide (MO) then accumulation of sulphates on the catalyst surface results to blockage of active sites and profound reduction of catalytic activity. This is probably the case for the

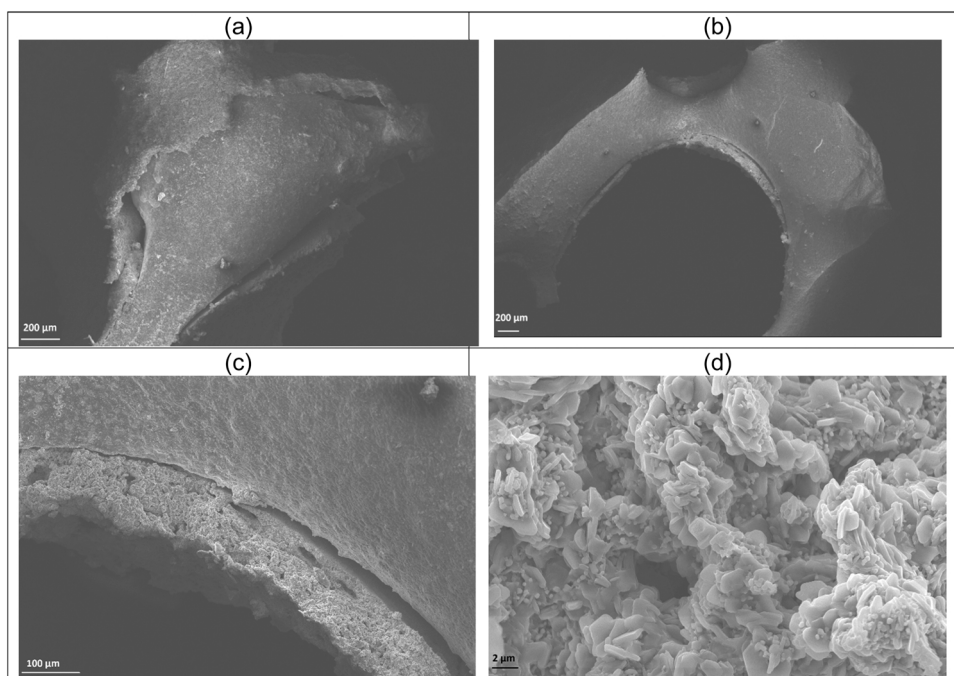


**Fig. 12.** SEM photographs of typical  $\text{Fe}_2\text{O}_3$ -coated SiSiC foam after 362 h on-stream exposure: (a), (b), (c) lower magnifications showing the morphology of the coated foam and of the SiSiC support-coating interface; (d) higher magnification on the catalyst coating showing its characteristic morphology with large elongated formations and smaller quasi-spherical particles.

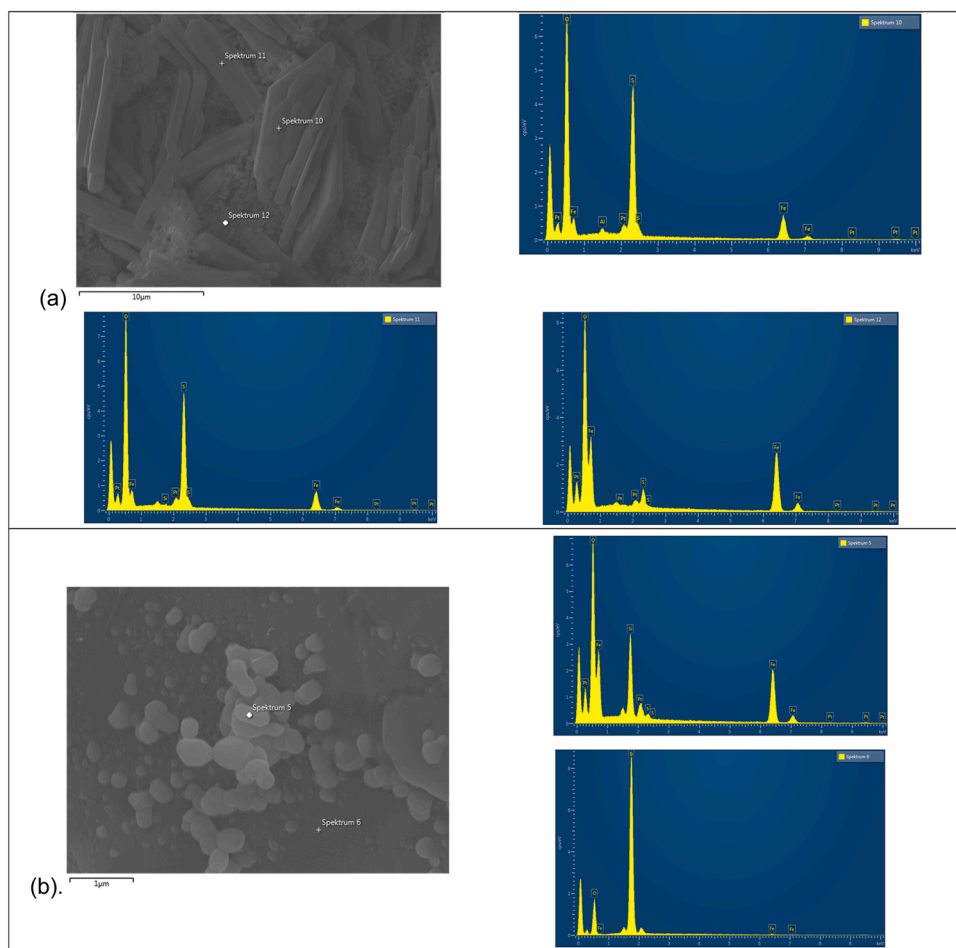


**Fig. 13.** SEM photographs under higher magnification and EDS microanalysis of the  $\text{Fe}_2\text{O}_3$ -coated SiSiC foam after 362 h on-stream exposure, shown in Fig. 12(a) characteristic surface morphology of the coating with large elongated formations and smaller quasi-spherical particles and respective EDS spectra at characteristic points indicated, showing clearly presence of sulphur, iron and oxygen at the former and lack of sulphur at the latter; (b) higher magnification on an area at the center of image (a) containing only quasi-spherical particles and respective EDS spectra at two characteristic points, showing clearly the elements of iron oxide on the particles and of SiSiC on the support, respectively.

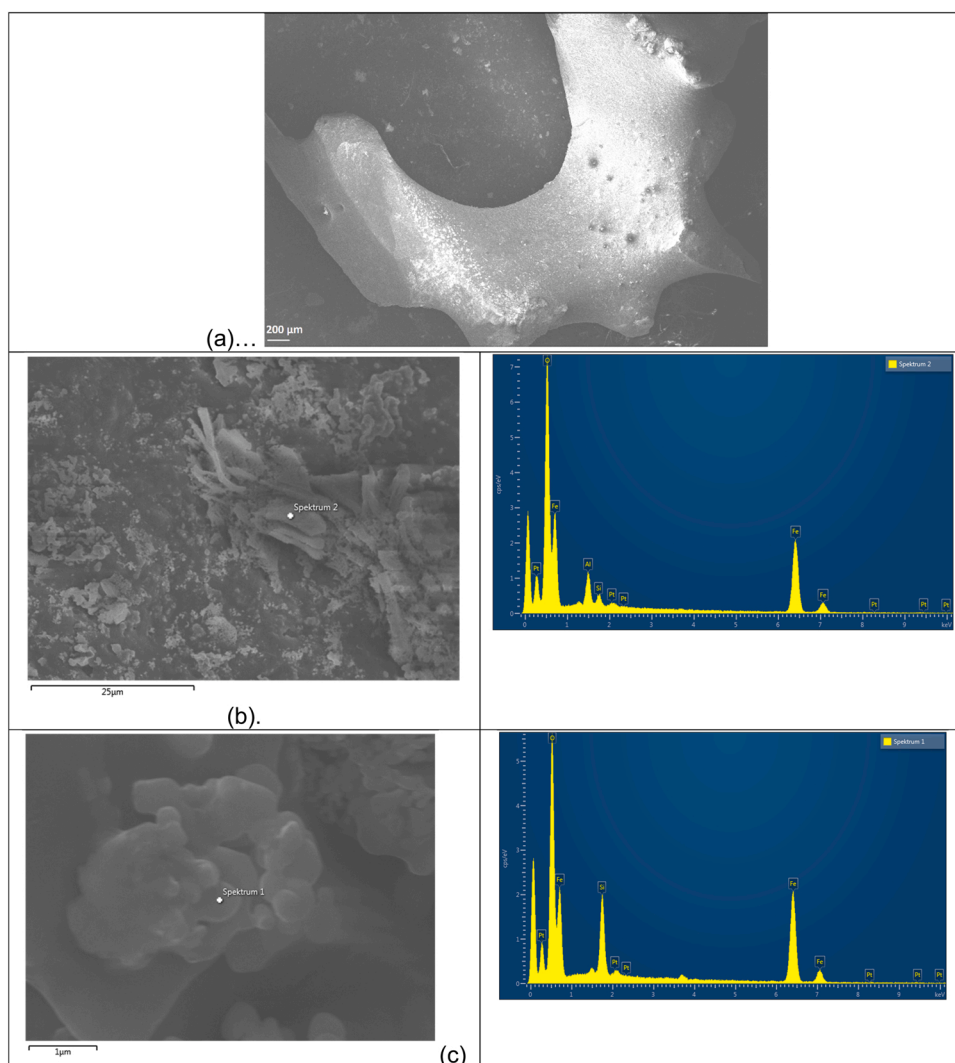


**Fig. 14.** SEM photographs of typical  $\text{Fe}_2\text{O}_3$ -coated SiSiC foam after on-stream exposure for 362 h and post-reaction TGA under air: (a) “strut-scale” magnification; (b) characteristic surface morphology of the coating observed under higher magnification and respective spectrum of elemental EDS microanalysis at the point indicated, demonstrating the absence of elemental sulphur on the particle’s surface; (c) higher magnification and EDS spectrum of another area of (b) containing only small, spherical-like particles, showing the same.

experiments under the higher flow rates tested in this study ( $V_{\text{H}_2\text{SO}_4} = 0.50 \text{ ml/min}$ ), leading to the observed deactivation with increasing time on stream under these flow rates. On the other hand, for the lowest flow rate ( $V_{\text{H}_2\text{SO}_4} = 0.10 \text{ ml/min}$ ) this balance is most likely achieved; i.e. an adequate number of catalytically active sites are sulphated but the dissociation of formed sulphates matches the rate of  $\text{SO}_3$  feed leading to a stable and relatively high conversion rate. Furthermore, it is also expected that the rate is affected both by the active surface area (i.e. catalytic dispersion which is actually quite high for the case of foams) and by sintering; i.e. the higher the sintering the lower the sulphate dissociation rate becomes and hence the easier the blockage of active sites.

### 3.4. Preparation and characterisation of iron oxide-coated foams

Based on the results above, the catalytic system to be incorporated in the sulphuric acid splitting reactor zone for the proof-of-concept demonstration validation, was selected to be comprised of foams coated with an inexpensive, yet active catalyst, like  $\text{Fe}_2\text{O}_3$ . This choice facilitates furthermore the construction of the entire sulphuric acid dissociation/sulphur trioxide splitting cascade solely from foams, non-coated and coated, respectively.

Work by CERTH involved the catalyst bed preparation which consisted of iron oxide-coated SiSiC foams with dimensions of  $\varnothing 24 \text{ mm} \times 40 \text{ mm}$  (Fig. 15a). As already reported in Section 2, after the dip coating step the segments were dried (Fig. 15b) and the procedure was repeated

with these “green” bodies as many times needed (in the specific case typically on average 8 repetitions – Fig. 15d) to achieve the required loading, with the final step being the calcination of the coated segments under air at  $900^\circ\text{C}$  to adhere the coating (Fig. 15c). Although the reactor (see below) requires only 24 SiSiC foams, twice as many foams were prepared to be readily available as spare parts (in total 49 segments).

The effect of loading on the pressure drop during a variable air flow passing through the foams (coated vs. uncoated) was measured. The results (Fig. 15e) on the one hand do not show any significant increase of pressure drop in the case of the non-coated foams, obviously due to the foams’ “open” structure. Indeed, even for an extremely high air flow of  $100 \text{ l}\cdot\text{min}^{-1}$  (std), the maximum pressure drop induced by the uncoated specimen remained lower than 4 mbar. On the other hand, in the case of a segment with  $\sim 44 \text{ wt}\%$  loading (the maximum value recorded among the 49 segments prepared) the respective measured pressure drop value was  $< 8 \text{ mbar}$ . This very low value of pressure drop is a significant advantage of these structures, especially in the perspective of considering pressurized reactors for the implementation of the  $\text{SO}_3$  splitting step, as elaborated in the Introduction.

An average loading of the final SiSiC segments in the range of 40 wt % was selected as optimal based on both the catalytic and the pressure drop evolution results. The loading values achieved per SiSiC foam for the 24 segments are shown in Fig. 15f, whereas ten of these segments are shown in Fig. 15g. The average value of the loading among the 24 segments selected to be incorporated in the reactor, was 37.5 wt%.

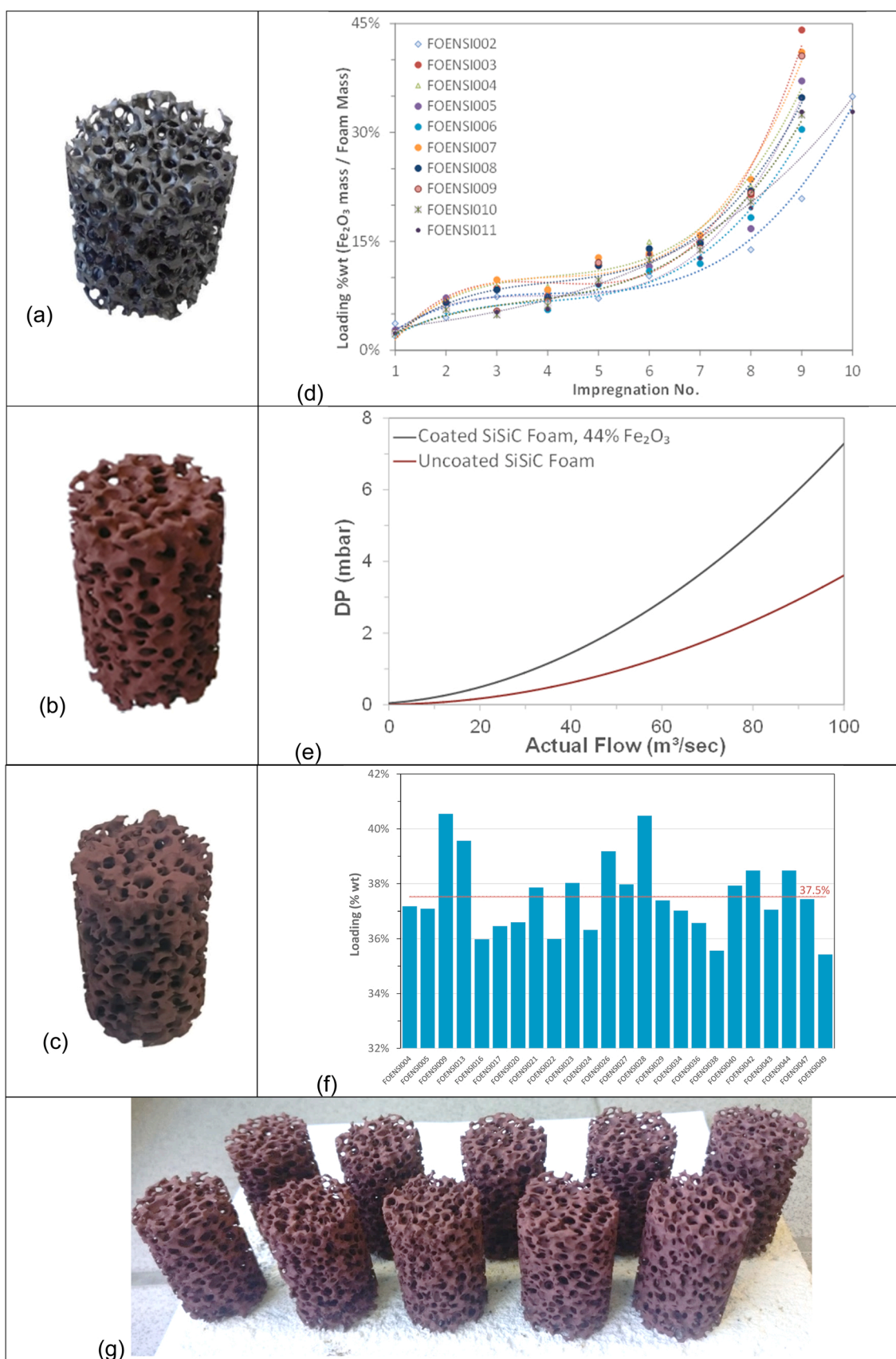


**Fig. 15.** Photographs of SiSiC foams at various process stages: (a) non-coated, (b) green (coated, non-calcined) and (c) calcined, coated segment with 38 wt %  $\text{Fe}_2\text{O}_3$  loading; (d) cumulative loading of 10 representative foams (calculated as mass of  $\text{Fe}_2\text{O}_3$  coating/mass of non-coated SiSiC support) per number of impregnations; (e) pressure drop evolution vs. applied air flow rate for non-coated and coated foams; (f) loading characteristics of 24 prepared SiSiC foams; (g) ten representative sintered coated segments.

### 3.5. Shell-and-tube catalytic reactor allothermally heated by a hot particles stream

In parallel, a proof-of-concept, 2 kW reactor/heat exchanger for sequential sulphuric acid dissociation/SO<sub>3</sub> splitting, comprised of six catalytic tubes designed to be heated through bauxite particles flowing in the shell through an electrically- heated inclined belt feeder was constructed at DLR [18]. Fig. 16a-e show CAD designs and actual photo-graphs of the reactor parts: shell, tubes manifold and catalytic structures screened in order to select the one to be eventually employed therein. The inner diameter of tubes is such to accommodate specimens of ~ 25 mm diameter like the ones employed in this work. The 24 Fe<sub>2</sub>O<sub>3</sub>-coated foams mentioned above are already installed in the reactor (4 per tube) together with a number of uncoated SiSiC foams and are currently being tested.

## 4. Conclusions

The present work involved the preparation and long-term testing of sulphur trioxide splitting structured catalytic systems, namely, honeycombs, foams and spherical particles. The rationale for the development and qualification of such systems emanates from the findings of our previous works that advocated for the implementation of the concentrated solar energy-driven combined sulphuric acid dissociation/SO<sub>3</sub> splitting endothermic step in non-moving catalytic bed structures allothermally heated by a moving bed of hot solid particles, previously directly irradiated in a centrifugal solar receiver. The concept is

applicable to all sulphur-based thermochemical cycles involving an SO<sub>3</sub> splitting step and thus can be employed for the production of “solar fuels” like either hydrogen or solid sulphur contributing to CO<sub>2</sub>-free energy supply.

Comparative sulphur trioxide splitting screening experiments with catalyst-coated SiSiC honeycombs for time periods between 100 and 950 h on-stream, demonstrated that Pt-based catalysts did not exhibit satisfactory conversion and suffered from deactivation with prolonged on-stream exposure times at 650 °C. This was attributed to extensive sulphation of the alumina support as determined with post-reaction (XRD and TGA) analysis. These drawbacks did not justify their higher cost at this developmental stage and thus emphasis was placed on the development of catalytic systems based on inexpensive iron oxide.

Structured catalysts involving iron oxide-coated SiSiC honeycombs and foams, as well as particles and foams made entirely of iron oxide were long-term tested with respect to their sulphur trioxide splitting capability. Parametric studies of such iron oxide catalytic systems with respect to sulphuric acid flow rate and reaction temperature were performed. Particle and foam structures made entirely of iron oxide did not exhibit satisfactory conversion, a fact attributed for the latter to the high sintering temperature required during their manufacture stage necessary to induce sufficient mechanical strength upon them. On the contrary, conversions close to equilibrium could be achieved at 850 °C with iron oxide-coated SiSiC foams, within a wide range of sulphuric acid flow rates. Furthermore, such foams exhibited very low pressure drop even under high catalyst loadings (35–45 wt%), an attribute that renders them suitable for pressurized operation as well.

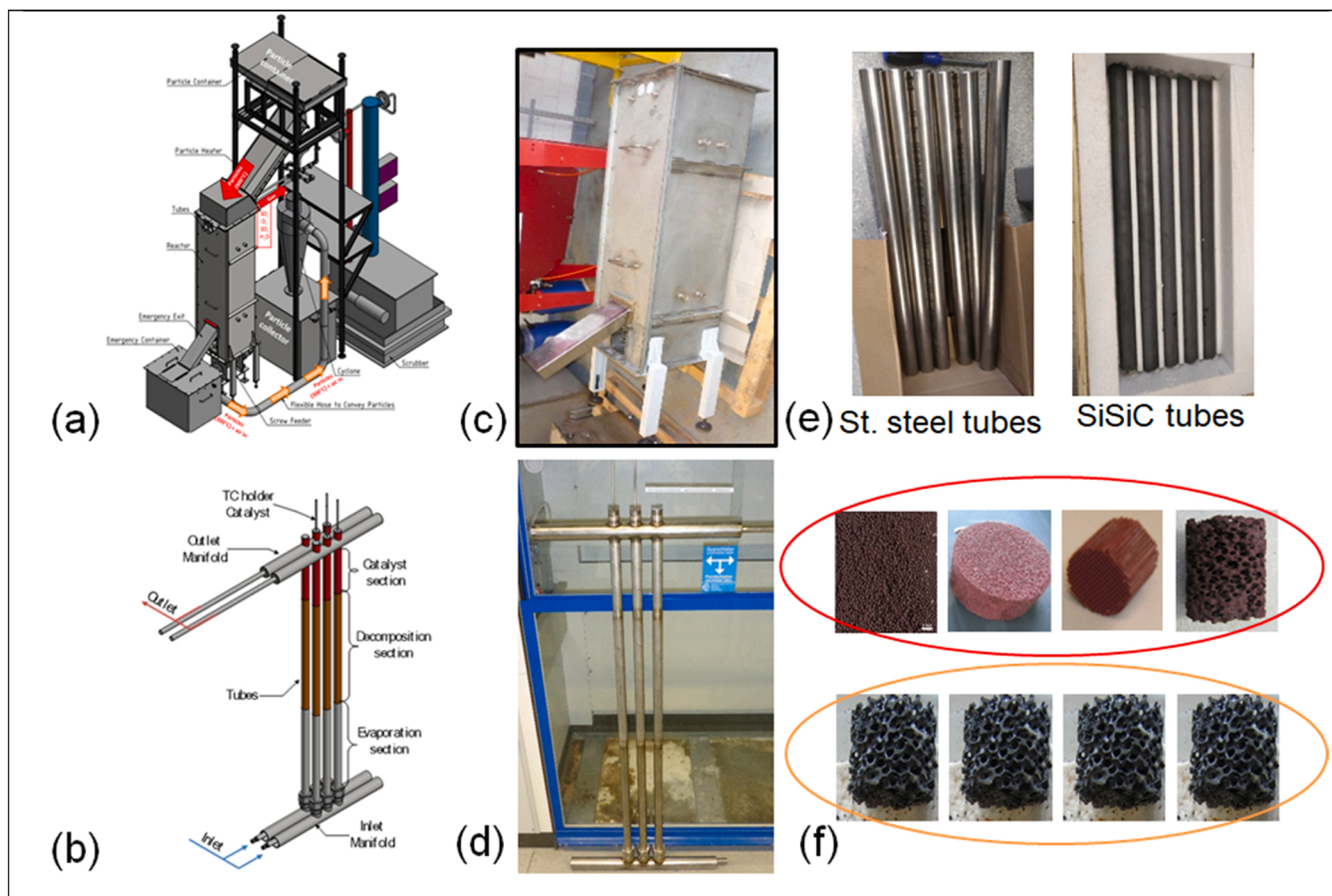


**Fig. 16.** (a), (b) CAD and 3D-models of lab-scale reactor/heat exchanger test setup and of the six reactor tubes included therein, respectively (from [18]); (c) actual reactor shell built with side safety exit gate for hot particles stream drain in case of emergency; (d) actual one of the two three-tubes manifold; each tube consists of (e) an outer stainless steel and an inner SiSiC tube, the latter coming into contact with the reactive gases; (f) Fe<sub>2</sub>O<sub>3</sub>-containing structures tested in the present work: from left to right: Fe<sub>2</sub>O<sub>3</sub>-made spherical particles (CERTH), Fe<sub>2</sub>O<sub>3</sub>-made foams (DLR), Fe<sub>2</sub>O<sub>3</sub>-coated SiSiC honeycombs and Fe<sub>2</sub>O<sub>3</sub>-coated SiSiC foams (CERTH) - the “lower”, non-catalytic H<sub>2</sub>SO<sub>4</sub> decomposition tubes section is comprised of non-coated SiSiC foams.

Based on these findings, a series of such catalytic iron oxide-coated SiSiC foams were prepared under a procedure optimized to result in reproducible loading. These structures have been incorporated in a proof-of-concept, 2 kW sulphuric acid dissociation/SO<sub>3</sub> splitting reactor/heat exchanger and are currently under testing, allothermally heated to the required reaction temperatures (> 800 °C) through an electrically-heated bauxite particles stream.

### CRedit authorship contribution statement

**Christos Agrafiotis:** Conceptualization, Methodology, Visualization, Project administration, Funding acquisition, Investigation, Writing - original draft, Writing - review & editing. **Dennis Thomey:** Project administration, Funding acquisition, Conceptualization, Formal analysis, Investigation, Methodology, Visualization, Writing - review & editing. **Lamark de Oliveira:** Investigation, Methodology, Validation. **George Karagiannakis:** Conceptualization, Methodology, Investigation, Visualization, Writing - review & editing, Project administration, Funding acquisition. **Nikolaos I. Tsongidis:** Investigation, Methodology, Validation, Visualization. **Chrysoula Pagkoura:** Investigation, Methodology, Validation, Visualization. **Gözde Alkan:** Resource. **Martin Roeb:** Resources, Funding acquisition, Supervision. **Christian Sattler:** Resources, Supervision.

### Declaration of Competing Interest

The authors declare that they have no known competing financial interests or personal relationships that could have appeared to influence the work reported in this paper.

### Data Availability

Data will be made available on request.

### Acknowledgement

This work was performed within the Project “PEGASUS: Power Generation by Solar Particle Receiver Driven Sulphur Storage Cycle”. The project has received funding from the European Union’s Horizon 2020 research and innovation programme under grant agreement No 727540.

### References

- [1] J.H. Norman, J.L. Russel, J.T. Porter, K.H. McCorkle, T.S. Roemer, R. Sharp, Process for the thermochemical production of hydrogen, US Patent No 4,089,940, Assignee General Atomics company, U.S, 1978.
- [2] L.E. Brecher, C.K. Wu, Electrolytic decomposition of water, Westinghouse Electric Corporation (Pittsburgh, PA), United States Patent 3888750, 1975.
- [3] J.H. Norman, Sulphuric Acid-Sulfur Heat Storage Cycle. US Patent 4,421,734, Assignee: General Atomics company, (San Diego, CA), United States, 1983.
- [4] B. Wong, L. Brown, R. Buckingham, W. Sweet, B. Russ, M. Gorenssek, Sulfur dioxide disproportionation for sulfur based thermochemical energy storage, *Sol. Energy* 118 (2015) 134–144.
- [5] C. Corgnale, M.B. Gorenssek, W.A. Summers, Review of sulfuric acid decomposition processes for sulfur-based thermochemical hydrogen production cycles, *Processes* 8 (2020) 1383.
- [6] A. Raj, S. Ibrahim, A. Jagannath, Combustion kinetics of H<sub>2</sub>S and other sulfurous species with relevance to industrial processes, *Prog. Energy Combust. Sci.* 80 (2020), 100848.
- [7] J.-G. Wagenfeld, K. Al-Ali, S. Almheiri, A.F. Slavens, N. Calvet, Sustainable applications utilizing sulfur, a by-product from oil and gas industry: A state-of-the-art review, *Waste Manag.* 95 (2019) 78–89.
- [8] C.W. Forsberg, Hydrogen, nuclear energy, and the advanced high-temperature reactor, *Int. J. Hydrog. Energ.* 28 (2003) 1073–1081.
- [9] Q. Sun, Q. Gao, P. Zhang, W. Peng, S. Chen, Modeling sulfuric acid decomposition in a bayonet heat exchanger in the iodine-sulfur cycle for hydrogen production, *Appl. Energy* 277 (2020), 115611.
- [10] H. Noguchi, H. Takegami, Y. Kamiji, N. Tanaka, J. Iwatsuki, S. Kasahara, S. Kubo, R&D status of hydrogen production test using IS process test facility made of industrial structural material in JAEA, *Int. J. Hydrog. Energ.* 44 (2019) 12583–12592.
- [11] H. Li, G. Tan, W. Zhang, S. Suppiah, Development of direct resistive heating method for SO<sub>3</sub> decomposition in the S–I cycle for hydrogen production, *Appl. Energy* 93 (2012) 59–64.
- [12] General Atomics, Decomposition of sulfuric acid using solar thermal energy, GA-A17573, General Atomics, 1985.
- [13] M. Roeb, D. Thomey, L. de Oliveira, C. Sattler, G. Fleury, F. Pra, P. Tochon, A. Brevet, G. Roux, N. Gruet, C. Mansilla, F. LeNaour, S. Poitou, R.W.K. Allen, R. Elder, G. Kargiannakis, C. Agrafiotis, A. Zygianni, C. Pagkoura, A. G. Konstandopoulos, A. Giaconia, S. Sau, P. Tarquini, S. Haussener, A. Steinfeld, I. Canadas, A. Orden, M. Ferrato, Sulphur based thermochemical cycles: development and assessment of key components of the process, *Int. J. Hydrog. Energ.* 38 (2013) 6197–6204.
- [14] C. Sattler, M. Roeb, C. Agrafiotis, D. Thomey, Solar hydrogen production via sulphur based thermochemical water-splitting, *Sol. Energy* 156 (2017) 30–47.
- [15] M. Ebert, L. Amsbeck, J. Rheinländer, B. Schlögl-Knothe, S. Schmitz, M. Sibus, R. Uhlig, R. Bock, Operational experience of a centrifugal particle receiver prototype, *AIP Conf. Proc.* 2126 (2019), 030018.
- [16] D.R. O’Keefe, J.H. Norman, D.G. Williamson, Catalysis research in the thermochemical water-splitting processes, *Catal. Rev. - Sci. Eng.* 22 (1980) 325–369.
- [17] C. Agrafiotis, D. Thomey, L. de Oliveira, M. Ebert, B. Gobreit, J. Perneptner, B. Schlögl-Knothe, G. Alkan, M. Roeb, C. Sattler, A particle receiver-driven thermochemical cycle employing elemental sulphur for solar thermochemical energy storage: investigation of particles as concentrated sunlight harvesting media and sulphur trioxide splitting catalysts, *Sol. Energy* 234 (2022) 21–38.
- [18] V.K. Thanda, D. Thomey, L. Mevißen, H. Noguchi, C. Agrafiotis, M. Roeb, C. Sattler, Solar thermochemical energy storage in elemental sulphur: design, development and construction of a lab-scale sulphuric acid splitting reactor powered by hot ceramic particles, *AIP Conf. Proc.* 2445 (2022).
- [19] D. Thomey, L. de Oliveira, J.-P. Säck, M. Roeb, C. Sattler, Development and test of a solar reactor for decomposition of sulphuric acid in thermochemical hydrogen production, *Int. J. Hydrog. Energ.* 37 (2012) 16615–16622.
- [20] S.S. Lin, R. Flaherty, Design studies of the sulfur trioxide decomposition reactor for the sulfur cycle hydrogen production process, *Int. J. Hydrog. Energ.* 8 (1983) 589–596.
- [21] G. Atomics, High-pressure catalytic metal reactor in a simulated solar central receiver, GA-A18285, General Atomics, 1986.
- [22] F. Gelbard, J.C. Andazola, G.E. Naranjo, C.E. Velasquez, A.R. Reay, High Pressure Sulfuric Acid Decomposition Experiments for the Sulfur-Iodine Thermochemical Cycle, Report SAND2005-5598, Sandia National Laboratories, 2005.
- [23] A. Cybulski, J.A. Moulijn, Structured Catalysts and Reactors, CRC Press, Boca Raton, FL, U.S.A., 2005.
- [24] D.M. Beall, W.A. Cutler, Smog begone! How development of ceramic automotive catalytic substrates and filters helped reduce air pollution, *Am. Ceram. Soc. Bull.* 99 (2020) 24–31.
- [25] C.C. Agrafiotis, I. Mavroidis, A.G. Konstandopoulos, B. Hoffschmidt, P. Stobbe, M. Romero, Q. ValerioFernandez, Evaluation of porous silicon carbide monolithic honeycombs as volumetric receivers/collectors of concentrated solar radiation, *Sol. Energy Mater. Sol. Cells* 91 (2007) 474–488.
- [26] J.H. Norman, K.J. Mysels, R. Sharp, D. Williamson, Studies of the sulfur-iodine thermochemical water-splitting cycle, *Int. J. Hydrog. Energ.* 7 (1982) 545–556.
- [27] H.A. Khan, A. Jaleel, E. Mahmoud, S. Ahmed, U.H. Bhatti, M. Bilal, Hussain, Development of catalysts for sulfuric acid decomposition in the sulfur-iodine cycle: a review, *Catal. Rev.* (2021) 1–36.
- [28] S. Pathak, S. Saini, K. Kondamudi, S. Upadhyayula, S. Bhattacharya, Insights into enhanced stability and activity of silica modified SiC supported iron oxide catalyst in sulfuric acid decomposition, *Applied Catalysis B: Environmental* (2020) 119613.
- [29] A. Nadar, A.M. Banerjee, M. Pai, S.S. Meena, A. Patra, P. Sastry, R. Singh, M. Singh, A. Tripathi, Immobilization of crystalline Fe<sub>2</sub>O<sub>3</sub> nanoparticles over SiO<sub>2</sub> for creating an active and stable catalyst: a demand for high temperature sulfuric acid decomposition, *Appl. Catal. B: Environ.* 283 (2021), 119610.
- [30] S. Tomar, S. Gangwar, K. Kondamudi, S. Upadhyayula, SO<sub>3</sub> decomposition over β-SiC and SiO<sub>2</sub> supported CuFe<sub>2</sub>O<sub>4</sub>: a stability and kinetic study, *Int. J. Hydrog. Energ.* 45 (2020) 21287–21296.
- [31] A. Banerjee, M. Pai, K. Bhattacharya, A. Tripathi, V. Kamble, S. Bharadwaj, S. Kulshreshtha, Catalytic decomposition of sulfuric acid on mixed Cr/Fe oxide samples and its application in sulfur-iodine cycle for hydrogen production, *Int. J. Hydrog. Energ.* 33 (2008) 319–326.
- [32] G. Karagiannakis, C.C. Agrafiotis, C. Pagkoura, A.G. Konstandopoulos, D. Thomey, L. de Oliveira, M. Roeb, C. Sattler, Hydrogen production via sulfur-based thermochemical cycles: Part 3: durability and post-characterization of silicon carbide honeycomb substrates coated with metal oxide-based candidate catalysts for the sulfuric acid decomposition step, *Int. J. Hydrog. Energ.* 37 (2012) 8190–8203.
- [33] S. Sujeesh, V.N. Ahmed, H. Fani, A.S. Rao, S. Mukhopadhyay, Kinetic study and modeling of sulphuric acid decomposition using Cr-Fe<sub>2</sub>O<sub>3</sub> catalyst for sulphur based water splitting processes, *Int. J. Hydrog. Energ.* 46 (2021) 27282–27292.
- [34] T. Kawada, T. Tajiri, H. Yamashita, M. Machida, Molten copper hexaaxodivanadate: an efficient catalyst for SO<sub>3</sub> decomposition in solar thermochemical water splitting cycles, *Catal. Sci. Technol.* 4 (2014) 780–785.
- [35] M. Machida, A. Ikematsu, A.S. Nur, H. Yoshida, Catalytic SO<sub>3</sub> decomposition activity of SiO<sub>2</sub>-supported alkaline earth vanadates for solar thermochemical water splitting cycles, *ACS Appl. Energy Mater.* (2021).
- [36] A.S. Nur, A. Ikematsu, H. Yoshida, M. Machida, Effects of coexisting oxoanions on SO<sub>3</sub> decomposition activity of molten-phase potassium metavanadate catalysts, *J. Ceram. Soc. Jpn.* 130 (2022) 107–112.

- [37] A. Christodoulakis, S. Boghosian, Molecular structure of supported molten salt catalysts for SO<sub>2</sub> oxidation, *J. Catal.* 215 (2003) 139–150.
- [38] I. Giakoumelou, V. Parvulescu, S. Boghosian, Oxidation of sulfur dioxide over supported solid V<sub>2</sub>O<sub>5</sub>/SiO<sub>2</sub> and supported molten salt V<sub>2</sub>O<sub>5</sub>-Cs<sub>2</sub>SO<sub>4</sub>/SiO<sub>2</sub> catalysts: molecular structure and reactivity, *J. Catal.* 225 (2004) 337–349.
- [39] A.M. Banerjee, M.R. Pai, R. Tewari, N. Raj, A.K. Tripathi, S.R. Bharadwaj, D. Das, A comprehensive study on Pt/Al<sub>2</sub>O<sub>3</sub> granular catalyst used for sulfuric acid decomposition step in sulfur-iodine thermochemical cycle: changes in catalyst structure, morphology and metal-support interaction, *Appl. Catal. B: Environ.* 162 (2015) 327–337.
- [40] A.M. Banerjee, A.R. Shirole, M.R. Pai, A.K. Tripathi, S.R. Bharadwaj, D. Das, P. K. Sinha, Catalytic activities of Fe<sub>2</sub>O<sub>3</sub> and chromium doped Fe<sub>2</sub>O<sub>3</sub> for sulfuric acid decomposition reaction in an integrated boiler, preheater, and catalytic decomposer, *Appl. Catal. B: Environ.* 127 (2012) 36–46.
- [41] S. Sujeesh, V.N. Ahmed, A.S. Rao, S. Mukhopadhyay, Sulphuric acid decomposition using Cr-Fe<sub>2</sub>O<sub>3</sub> catalyst in a tubular packed bed reactor (PBR): modeling and experimental studies, *Int. J. Hydrog. Energ.* 47 (2022) 11750–11763.
- [42] W. Liu, W.P. Addiego, C.M. Sorensen, T. Boger, Monolith reactor for the dehydrogenation of ethylbenzene to styrene, *Ind. Eng. Chem. Res.* 41 (2002) 3131–3138.
- [43] W.P. Addiego, W. Liu, T. Boger, Iron oxide-based honeycomb catalysts for the dehydrogenation of ethylbenzene to styrene, *Catal. Today* 69 (2001) 25–31.
- [44] N.I. Tsongidis, G. Karagiannakis, K.G. Sakellariou, C. Pagkoura, A. G. Konstandopoulos, Iron Oxide-Based Particles for High Temperature Thermochemical Energy Storage via the Elemental Sulfur Thermochemical Cycle. AIP Conference Proceedings, AIP Publishing LLC., 2019, 210009.
- [45] C. Agrafiotis, D. Thomey, L. de Oliveira, N. Overbeck, V.K. Thanda, M. Roeb, C. Sattler, Solar Energy Conversion and Storage through Sulphur-Based Thermochemical Cycles Implemented on Centrifugal Particle Receivers AIP Conference Proceedings, 2303 (2020).
- [46] C. Agrafiotis, T. Block, M. Senholdt, S. Tescari, M. Roeb, C. Sattler, Exploitation of thermochemical cycles based on solid oxide redox systems for thermochemical storage of solar heat. Part 6: testing of Mn-based combined oxides and porous structures, *Sol. Energy* 149 (2017) 227–244.
- [47] S. Pathak, S. Upadhyayula, A review on the development of supported non-noble metal catalysts for the endothermic high temperature sulfuric acid decomposition step in the Iodine-Sulfur cycle for hydrogen production, *Int. J. Hydrog. Energ.* (2022).
- [48] G. Karagiannakis, C.C. Agrafiotis, A. Zygogianni, C. Pagkoura, A. G. Konstandopoulos, Hydrogen production via sulfur-based thermochemical cycles: Part 1: synthesis and evaluation of metal oxide-based candidate catalyst powders for the sulfuric acid decomposition step, *Int. J. Hydrog. Energ.* 36 (2011) 2831–2844.
- [49] C. Agrafiotis, D. Thomey, L. de Oliveira, C. Happich, M. Roeb, C. Sattler, N. I. Tsongidis, K.G. Sakellariou, C. Pagkoura, G. Karagiannakis, A. G. Konstandopoulos, D. Pomykalska, M. Zagaja, D. Janus, Oxide particles as combined heat storage medium and sulphur trioxide decomposition catalysts for solar hydrogen production through sulphur cycles, *Int. J. Hydrog. Energ.* 44 (2019) 9830–9840.
- [50] A. Giaconia, S. Sau, C. Felici, P. Tarquini, G. Karagiannakis, C. Pagkoura, C. Agrafiotis, A.G. Konstandopoulos, D. Thomey, L. de Oliveira, M. Roeb, C. Sattler, Hydrogen production via sulfur-based thermochemical cycles: Part 2: performance evaluation of Fe<sub>2</sub>O<sub>3</sub>-based catalysts for the sulfuric acid decomposition step, *Int. J. Hydrog. Energ.* 36 (2011) 6496–6509.
- [51] D.M. Ginosar, H.W. Rollins, L.M. Petkovic, K.C. Burch, M.J. Rush, High-temperature sulfuric acid decomposition over complex metal oxide catalysts, *Int. J. Hydrog. Energ.* 34 (2009) 4065–4073.
- [52] D.M. Ginosar, L.M. Petkovic, A.W. Glenn, K.C. Burch, Stability of supported platinum sulfuric acid decomposition catalysts for use in thermochemical water splitting cycles, *Int. J. Hydrog. Energ.* 32 (2007) 482–488.
- [53] H.A. Khan, P. Natarajan, K.-D. Jung, Stabilization of Pt at the inner wall of hollow spherical SiO<sub>2</sub> generated from Pt/hollow spherical SiC for sulfuric acid decomposition, *Appl. Catal. B: Environ.* 231 (2018) 151–160.
- [54] H.A. Khan, K.-D. Jung, Preparation scheme of active Pt/SiC catalyst and its phase changes during sulfuric acid decomposition to produce hydrogen in the SI cycle, *Catal. Lett.* 147 (2017) 1931–1940.
- [55] C. Agrafiotis, A. Tsetsekou, I. Leon, Effect of slurry rheological properties on the coating of ceramic honeycombs with Yttria-Stabilized-Zirconia washcoats, *J. Am. Ceram. Soc.* 83 (2000) 1033–1038.
- [56] M.V. Twigg, J.T. Richardson, Fundamentals and applications of structured ceramic foam catalysts, *Ind. Eng. Chem. Res.* 46 (2007) 4166–4177.
- [57] T. Fend, O. Reutter, R. Pitz-Paal, B. Hoffschmidt, Cellular Ceramics Use in Solar Radiation Conversion, in: M. Scheffler, P. Colombo (Eds.), *Cellular Ceramics: Structure, Manufacturing, Properties and Applications*, John Wiley-VCH, Weinheim, 2005, pp. 523–546.
- [58] T. Fend, B. Hoffschmidt, R. Pitz-Paal, O. Reutter, P. Rietbrock, Porous materials as open volumetric solar receivers: experimental determination of thermophysical and heat transfer properties, *Energy* 29 (2004) 823–833.